Universality in the mean spatial shape of avalanches

Thimothée Thiery and Pierre Le Doussal

CNRS-Laboratoire de Physique Théorique de l'Ecole Normale Supérieure, 24 rue Lhomond,75231 Cedex 05, Paris, France
(Dated: January 5, 2016)

Quantifying the universality of avalanche observables beyond critical exponents is of current great interest in theory and experiments. Here, we improve the characterization of the spatio-temporal process inside avalanches in the universality class of the depinning of elastic interfaces in random media. Surprisingly, at variance with the temporal shape, the spatial shape of avalanches has not yet been predicted. In part this is due to a lack of an analytically tractable definition: how should the shapes be centered? Here we introduce such a definition, accessible in experiments, and study the *mean spatial shape of avalanches at fixed size centered around their starting point (seed)*. We calculate the associated universal scaling functions, both in a mean-field model and beyond. Notably, they are predicted to exhibit a cusp singularity near the seed. The results are in good agreement with a numerical simulation of an elastic line.

PACS numbers:

Numerous slowly driven non-linear systems exhibit motion which is not smooth in time but rather proceeds discontinuously via jumps extending over a broad range of space and time scales. Developing predictive models of avalanche motion and understanding their universality, or lack thereof, has emerged as an outstanding challenge of modern statistical physics [1]. In condensed matter recent developments have led to distinguish two broad classes, depending on the importance of plastic deformations. In systems such as dislocated solids, metallic glasses, granular media near jamming, the latter play a crucial role and despite recent progresses a theoretical description is still under construction [2–5]. In many other situations the description by an elastic interface driven in a disordered medium has proved relevant [6–9]. Examples are domain walls in soft magnets [10, 11], fluid contact lines on rough surfaces [12, 13], strike-slip faults in geophysics [14], fractures in brittle materials [15–18] or imbibition fronts [19]. This class exhibits a dynamical phase transition - the so-called depinning transition - accompanied by collective avalanche motion. While the microscopic details of the dynamics are specific to each system, the large scale statistical properties of the avalanches are believed to be universal. The most studied quantities in this context are the critical exponents characterizing the scale-free probability distribution function (PDF) of avalanche total sizes S, $P(S) \sim S^{-\tau_S}$ and durations T, $P(T) \sim T^{-\tau_T}$. They are related to the roughness and dynamical exponents, ζ and z, defined at the depinning transition of the interface, using the scaling relations $S \sim \ell^{d+\zeta}$ and $T \sim \ell^z$ with ℓ the lateral extension of the avalanche.

Recent improvements in experimental techniques allow to study avalanches with higher accuracy and to access new, finer quantities, with the aim of distinguishing more efficiently the different universality classes. This notably includes the direct imaging of the spatio-temporal process of the velocity field inside an avalanche $v(x,t)$ where x denotes the internal coordinate of the (d-dimensional) interface and t is the time since the beginning of the
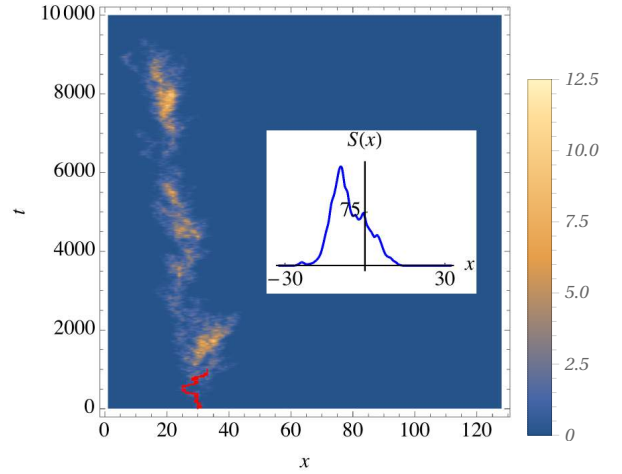

FIG. 1: Density plot of the velocity field $v(x,t)$ inside an avalanche of size $S = 1760$ in the mean-field model (BFM) for $d = 1$ discretized with $N = 128$ points. Time is given in machine-time unit. Line in red: backward path produced by the algorithm used to find the seed of the avalanche (see text). Inset: the spatial shape of this avalanche when centered around its starting point.

avalanche. A question of great interest is to understand whether and how scaling and universality extend to $v(x,t)$. Until now the focus was on the center of mass velocity $v_{\mathrm{cm}}(t) \sim \int d^d x \ v(x,t)$ and the mean temporal shape at fixed duration T, $\langle v_{\mathrm{cm}}(t) \rangle_T$. A scaling analysis suggests, through the sum rule $S = \int dt d^d x v(x,t)$, the existence of a scaling function $f_d^{\mathrm{temp}}(t)$ such that $\langle v_{\mathrm{cm}}(t) \rangle_T = T^{\gamma-1} f_d^{\mathrm{temp}}(t/T)$, where $\gamma = (d+\zeta)/z$. The universality of $f_d^{\mathrm{temp}}(t)$ was shown theoretically and studied experimentally in [20–23]. The beautiful parabola-shape predicted at mean field level, $f_{\mathrm{temp}}(t) = t(1 - t)$ (and $\gamma = 2$), stimulated the excitement around this observable.

Though very interesting, this observable does not contain information on the remarkable spatial structure of

avalanche processes (see for illustration Fig. 1). A characterization of even the mean spatial shape of avalanches in terms of a simple scaling function is presently lacking. In this Letter we propose and calculate such a scaling function. We consider the mean shape of avalanches at fixed total size S, for which a scaling analysis suggests (in real or in Fourier space $\langle S(q) \rangle_S = \int d^d x e^{iqx} \langle S(x) \rangle_S$)

$$\langle S(x) \rangle_S = S^{1 - \frac{d}{d+\zeta}} f_d(\frac{x}{S^{\frac{1}{d+\zeta}}})$$

$$\langle S(q) \rangle_S = S \tilde{f}_d(q S^{\frac{1}{d+\zeta}}) \tag{1}$$

where $S(x) = \int dt \, v(x,t)$ is the "local size" at x, $f_d(x)$ and $\tilde{f}_d(q)$ are radial scaling functions, normalized as $\int d^d x f_d(x) = \tilde{f}_d(q = 0) = 1$, since $S = \int d^d x \, S(x)$. Note that these definitions are not complete: there are various ways of centering an avalanche. Our proposal is to study the spatial structure by *centering the avalanches on their starting points.* We call this procedure the *seed-centering* which appears natural when one thinks of how an avalanche unfolds following a branching process (see Fig. 1). Furthermore, it permits analytical treatment and is thus appropriate to compare theory and experiments.

We first calculate the above scaling functions at the level of mean-field. This requires to go beyond the simplest mean-field toy model, the ABBM model [24, 25] which only describes the center of mass motion of the interface. To this aim we consider the Brownian Force Model (BFM), recently introduced as the relevant mean-field theory to describe spatial correlations [26–29]. For this model, we even compute the full *mean velocity-field inside a seed-centered avalanche of given size S* which in general obeys the scaling form

$$\langle v(x,t) \rangle_S = S^{\frac{\zeta - z}{d + \zeta}} F(t/S^{\frac{z}{d+\zeta}}, x/S^{\frac{1}{d+\zeta}}) \, . \tag{2}$$

More generally, in this Letter we consider elastic interfaces in the quenched Edward-Wilkinson universality class with short ranged disorder. In this context, the BFM is accurate for $d \geq d_c$, where d_c is the upper critical dimension of the depinning transition, $d_c = 4$ for short-range (SR) elasticity and $d_c = 2$ for the most common long-range (LR) elasticity. In lower dimensions $d < d_c$, correlations play an important role. To take them into account and study this more difficult case, we use the Functional Renormalization Group (FRG) and calculate the scaling functions $f_d(x)$ and $\tilde{f}_d(q)$ perturbatively in $\epsilon = d_c - d$, to one-loop, i.e. $O(\epsilon)$ accuracy (see [30–33] for background on FRG, and [26, 29, 34, 35] for its application to the study of avalanches). We show that the scaling ansatz (1) holds and that the scaling functions contain only one non-universal scale ℓ_σ (which is discussed in details below)

$$f_d(x) = \frac{1}{\ell_\sigma^d} \mathcal{F}_d(\frac{x}{\ell_\sigma}) \quad , \quad \tilde{f}_d(q) = \tilde{\mathcal{F}}_d(\ell_\sigma q) \tag{3}$$

where $\mathcal{F}_d$ and $\tilde{\mathcal{F}}_d$ are fully universal and depend only on the space dimension d and the universality class of the
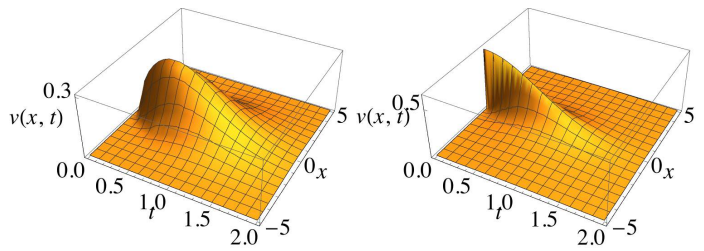

FIG. 2: Plot of the mean-field result for the space-time mean velocity profile inside an avalanche in $d = 1$ for SR (left, see (4)) and LR elasticity (right, see (7)).

model (i.e. range of elasticity and disorder). We now describe our main results, and report the discussion of the model and methods in the second part of the Letter.

Results within mean-field: The BFM model can be studied analytically in any dimension d. Let us first consider the case of SR elasticity. The exponents are $\tau_S = 3/2$, $\tau_T = z = 2$ and $\zeta = 4 - d$. The scaling function in (2) admits a very simple expression:

$$F(t,x) = 2t e^{-t^2} \frac{1}{(4\pi t)^{d/2}} e^{-x^2/(4t)} \tag{4}$$

which is plotted in Fig. 2. Here we use dimensionless units, the original units can be recovered using $x \to mx$, $t \to t/\tau_m$ and $S \to S/S_m$ where $\tau_m = \eta/m^2$ and $S_m = \sigma/m^4$ and the parameters η, m and σ are those in the equation of motion of the model (12). Time integration of (4) confirms for the BFM the general scaling law (1) and (3) with $\mathcal{F}_d^{\mathrm{MF}}(x) = \int_0^{+\infty} dt F(t,x)$ and $\ell_\sigma = \sigma^{-1/4}$. The result is simplest in Fourier space and does not depend on the dimension:

$$\tilde{\mathcal{F}}_d^{\mathrm{MF}}(q) = \tilde{\mathcal{F}}^{\mathrm{MF}}(q) = 1 - \frac{\sqrt{\pi} q^2}{2} e^{\frac{q^4}{4}} \mathrm{erfc}\left(\frac{q^2}{2}\right) \tag{5}$$

where $\mathrm{erfc}(z) = \frac{2}{\sqrt{\pi}} \int_z^{+\infty} e^{-t^2}$. In real space, $\mathcal{F}_d^{\mathrm{MF}}(x)$ depends on the dimension and can be expressed using hypergeometric functions [36] with $\mathcal{F}_{d \leq 4}^{\mathrm{MF}}(0) = \frac{2^{-d} \pi^{1 - \frac{d}{2}}}{\Gamma(\frac{d}{4}) \sin(\frac{\pi d}{4})}$. Both $\tilde{\mathcal{F}}^{\mathrm{MF}}(q)$ and $\mathcal{F}_{d=1,2}^{\mathrm{MF}}(x)$ are plotted in black in Fig. 3. A fundamental property of $\tilde{\mathcal{F}}^{\mathrm{MF}}(q)$ is that it possesses an algebraic tail $\tilde{\mathcal{F}}^{\mathrm{MF}}(q) \sim q^{-4}$ at large q, which generates a non-analytic term $\sim |x|^{4-d}$ in the small x expansion of $\mathcal{F}_d^{\mathrm{MF}}(x)$ around the origin. Its behavior at large x is evaluated using a saddle-point on (4), leading to a stretched exponential decay with a d-independent exponent 4/3:

$$\mathcal{F}_d^{\mathrm{MF}}(x) \simeq_{x \to \infty} \frac{2^{-d/2} \pi^{\frac{1}{2} - \frac{d}{2}}}{\sqrt{3}} x^{\frac{2-d}{3}} e^{-\frac{3 x^{4/3}}{4}} \, . \tag{6}$$

These results easily extend to LR elasticity, in which case $z = 1$, $\zeta = 2 - d$ and the mean shape in Fourier space is obtained replacing $q^2 \to q$ in (5). Let us also give here the spatiotemporal shape (2) for the experimentally most

relevant case of $d = 1$, with

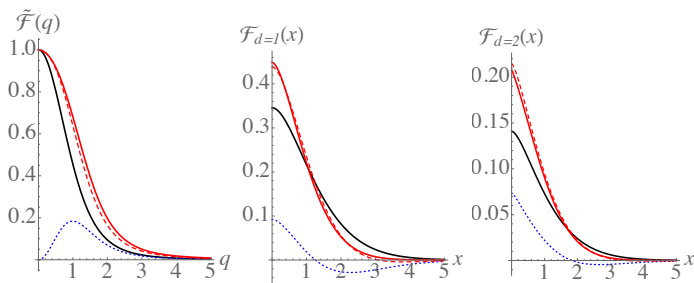$$F(t, x) = \frac{2t^2 e^{-t^2}}{\pi(x^2 + t^2)} \ . \tag{7}$$

FIG. 3: Analytical results at MF and $O(\epsilon)$ level for the universal scaling function $\tilde{\mathcal{F}}_{d=1}$ in Fourier space (Left) and $\mathcal{F}_d$ in real space for $d = 1$ (Middle) and $d = 2$ (Right) for SR elasticity. Black lines: tree/mean-field results. Dotted blue lines: universal corrections, $\delta\tilde{\mathcal{F}}_1(q)$ (left, $O(\epsilon)$ correction in Fourier space in $d = 1$), $\delta\mathcal{F}_1(x)$ (middle) and $\delta\mathcal{F}_2(x)$ (right). Red-dashed lines: $O(\epsilon)$ estimate obtained by simply adding the corrections to the MF value. Red lines: improved $O(\epsilon)$ estimate, which, through a re-exponentiation procedure, takes properly into account the modification of exponents (10) and (11) (see [36]).

Results beyond mean-field for SR elasticity: For realistic SR disorder, the BFM is the starting point in the $\epsilon = 4 - d$ expansion. It is most clearly implemented in Fourier space, since the mean-field result for $\tilde{\mathcal{F}}_d(q)$ does not depend on d:

$$\tilde{\mathcal{F}}_d^{\mathrm{SR}}(q) = \tilde{\mathcal{F}}^{\mathrm{MF}}(q) + \delta\tilde{\mathcal{F}}_d(q) + O(\epsilon^2) \tag{8}$$

with $\delta\tilde{\mathcal{F}}_d(q) = \epsilon\tilde{\mathcal{F}}^{(1)}(q)$. Here $\tilde{\mathcal{F}}^{(1)}(q) = \int_{\mathcal{C}} \frac{d\mu}{2i\pi} e^{\mu} \tilde{H}(\mu, q)$ is obtained as an Inverse Laplace Transform (ILT) $\mu \to 1$:

$$\tilde{H}(\mu, q) = \frac{4\sqrt{\pi}}{9} \left[\frac{2 - 3\gamma_E}{8} \frac{1}{q^2 + 2\sqrt{\mu}} - \frac{4\sqrt{\mu}}{(q^2 + 2\sqrt{\mu})^2} \right. \tag{9}$$

$$\left. \times \left(\frac{q^2 + 9\sqrt{\mu}}{q\sqrt{q^2 + 8\sqrt{\mu}}} \sinh^{-1}\left(\frac{q}{2\sqrt{2\sqrt{\mu}}} \right) - 1 + \frac{3}{16}\ln(4\mu) \right) \right]$$

where γ_E is Euler's Gamma constant (see [36] for the choice of $\mathcal{C}$). We then define the correction to the mean shape in real space as the d-dimensional Fourier transform $\delta\mathcal{F}_d(x) = \int \frac{d^d q}{(2\pi)^d} e^{-iqx} \delta\tilde{\mathcal{F}}_d(q)$. Hence, $\mathcal{F}_d^{\mathrm{SR}}(x) = \mathcal{F}_d^{\mathrm{MF}}(x) + \delta\mathcal{F}_d(x) + O(\epsilon^2)$. From the ILT expression (9) we obtain the following analytical properties of the $O(\epsilon)$ corrections:

1) Its large q expansion is $\delta\tilde{\mathcal{F}}_d(q) \simeq_{q\gg1} \epsilon\frac{8\log(q)-\gamma_E-8}{9q^4}$, interpreted as a *change in the tail exponent* $\tilde{\eta}_d$

$$\tilde{\mathcal{F}}_d(q) \simeq_{q\gg1} \tilde{A}_d q^{-\tilde{\eta}_d} \quad , \quad \tilde{\eta}_d = 4 - \frac{4\epsilon}{9} + O(\epsilon^2) \tag{10}$$

with $A_d = 2(1 - (2 + \frac{\gamma_E}{4})\frac{2\epsilon}{9})$. In real space this implies, in the expansion of $\mathcal{F}_d(x)$ at small x, a non-analytic

term $\sim |x|^{\eta_d}$ with $\eta_d = \tilde{\eta}_d - d = \frac{5\epsilon}{9} + O(\epsilon^2)$. Restoring the S dependence from (1) this leads to $\langle S(q) \rangle_S \sim_{q\to+\infty} S^{1-\frac{\tilde{\eta}_d}{d+\zeta}} q^{-\tilde{\eta}_d}$ and the non-analytic part $\langle S(x) \rangle_S^{n.a} \sim_{x\to0} S^{1-\frac{\tilde{\eta}_d}{d+\zeta}} |x|^{\eta_d}$. Note that in the BFM the value $\tilde{\eta}_d = 4 = d + \zeta$ implies that the large q behavior of $\langle S(q) \rangle_S$ does *not depend on* S. This may seem natural: in the BFM the small scales do not know about the total size of the avalanche. A generalization of this property to the SR disorder case would suggest the guess $\tilde{\eta}_d^{\mathrm{guess}} = d + \zeta$. Our result explicitly shows that this property fails with $\tilde{\eta}_d > d + \zeta$. Hence in the SR model the *large avalanches tend to be more smooth than small avalanches.* Note that the predicted value of η_d is smaller than 2 in all physical dimension: *this non-analytic term should actually dominate the behavior of* $\mathcal{F}_d(x)$ *around* 0 (and thus lead to a cusp singularity).

2) At large x, we obtain that the stretched exponential decay exponent of the mean shape is modified from its MF behavior $\delta^{\mathrm{MF}} = 4/3$

$$\mathcal{F}_d(x) \sim e^{-Cx^\delta} \quad , \quad \delta = \frac{4}{3} + \frac{2}{27}\epsilon + O(\epsilon^2) \tag{11}$$

with $C = \frac{3}{4} + (\frac{7\sqrt{3}}{36} - 1)\frac{2}{9}\epsilon$. Remarkably, using $\zeta = \epsilon/3 + O(\epsilon^2)$, this agrees to $O(\epsilon)$ with the conjecture $\delta = \frac{d+\zeta}{d+\zeta-1}$ that we justify in [36].

Furthermore, the ILT expression (9) is easily calculated numerically. The corrections $\delta\tilde{\mathcal{F}}_d(q)$ and $\delta\mathcal{F}_d(x)$ are shown in Fig. 3, together with the resulting estimates for the functions $\mathcal{F}_d^{\mathrm{SR}}(x)$ and $\tilde{\mathcal{F}}_d^{\mathrm{SR}}(q)$.

Model and method: For SR elasticity, the equation of motion for the interface position $u(x, t)$ (denoted u_{xt}) is

$$\eta\partial_t u_{xt} = \nabla_x^2 u_{xt} - m^2(u_{xt} - w_{xt}) + F(u_{xt}, x) \tag{12}$$

where η is the friction, m is a mass cutoff which suppresses fluctuations beyond the length $\ell_m = 1/m$ and $m^2 w_{xt}$ is the driving force. In the BFM, the random pinning force $F(u, x)$ is an independent Brownian motion in u for each x with $\overline{(F(u, x) - F(u', x))^2} = 2\sigma|u - u'|$. For the SR universality class, the second cumulant is $\overline{F(u, x)F(u', x')} = \delta^d(x - x')\Delta_0(u - u')$ with $\Delta_0(u)$ a fast decaying function. Eq. (12) is analyzed using the dynamical field theory and the FRG [36]. This leads to an expression for $\langle S(x) \rangle_S$ as an ILT: $\langle S(y) \rangle_S \sim LT^{-1}_{\mu\to S}(\langle \tilde{u}^1_{x=0} \rangle_\xi)/\rho(S)$ where $\rho(S)$ is the avalanche-size density (previously computed to $O(\epsilon)$ accuracy in [29, 35]) and $\tilde{u}^1_{x=0}$ is the $O(\lambda)$ term taken at $x = 0$ of the solution $\tilde{u}_x$ of the following differential equation (here in dimensionless units):

$$-\mu + \lambda\delta(x - y) + (\tilde{u}_x)^2 + \nabla_x^2 \tilde{u}_x - (1 + \xi_x)\tilde{u}_x = 0 \tag{13}$$

where ξ_x is a white-noise of order $\sqrt{\epsilon}$ and $\langle . \rangle_\xi$ denotes the average over it. For the BFM, the result is thus obtained setting $\xi_x \to 0$ above. At $O(\epsilon)$ for the SR universality class, it is thus sufficient to solve (13) perturbatively to second order in ξ_x.

In our model (12), the non-universal scale ℓ_σ in (3) is $m^{-1}S_m^{-1/(d+\zeta)}$ where S_m is defined from the ratio of the first two moments of the avalanche size distribution, $S_m = \langle S^2\rangle/(2\langle S\rangle)$, which can be measured in numerics and experiments. In cases where the numerical or experimental setup corresponds to our model (as in our simulations, see below), this prediction for ℓ_σ allows unambiguous comparison between our results and the data. In cases where ℓ_σ cannot be predicted, some scale-independent features of the mean-shape still allow comparison with the experiments. This includes the tail exponent of $\tilde{\mathcal{F}}_d(q)$ in (10), the small and large distance behavior of $\mathcal{F}_d(x)$ in (11), and the *universal ratios* $c_p = \frac{\int d^dx |x|^{2p}\mathcal{F}_d(x)}{(\int d^dx |x|^p\mathcal{F}_d(x))^2}$. In $d=1$, $(c_1, c_2) \simeq (1.6944, 3.8197)$ for the BFM while $(c_1, c_2) \simeq (1.641 \pm 0.001, 3.43 \pm 0.02)$ for SR model to $O(\epsilon)$.
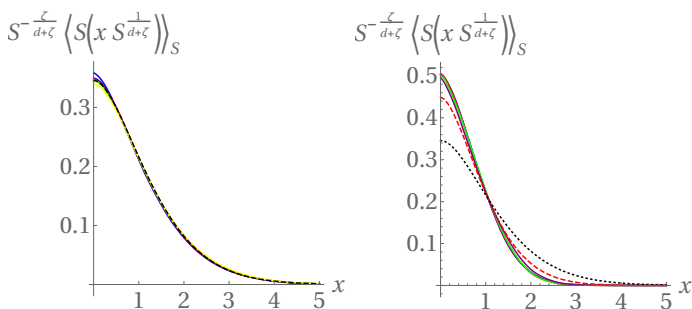

FIG. 4: Plain lines: rescaled mean shapes of avalanches at fixed size S from the simulation of the BFM model (left) and of the SR model (right), in $d=1$, for $S=10$ (left only, blue), $S=50$ (right only, blue), $S=10^2$ (red), $S=10^3$ (green), $S=10^4$ (purple) and $S=10^5$ (left only, yellow). Dashed black lines: theoretical MF result. Red dashed line: $O(\epsilon)$ result. No fitting parameter.

Numerical simulations. A convenient choice of SR disorder, amenable to Markovian evolution, is the Gaussian disorder $F(u,x)$ with "Ornstein-Uhlenbeck" (OU) correlator $\Delta_0(u) = \sigma\delta u e^{-|u|/\delta u}$. It is defined by two coupled equations for the velocity $v_{xt} \equiv v(x,t)$ and the force $\mathsf{F}(x,t)$

$$\eta\partial_t v_{xt} = \nabla^2 v_{xt} + m^2(\dot{w}_t - v_{xt}) + \partial_t\mathsf{F}(x,t)$$
$$\partial_t\mathsf{F}(x,t) = \sqrt{2\sigma v_{xt}}\chi_{xt} - \frac{v_{xt}}{\delta u}\mathsf{F}(x,t) \qquad (14)$$

with χ_{xt} a centered Gaussian white noise $\overline{\chi_{xt}\chi_{x't'}} = \delta^d(x-x')\delta(t-t')$ and initial condition $v_{xt=0} = \mathsf{F}(x,t=0) = 0$. In the stationary regime, this model is equivalent [39, 40] to Eq. (12) with $\dot{u}_{xt} = v_{xt}$ and $\mathsf{F}(x,t) = F(u_{xt},x)$ and initial condition $u_{xt=0} = 0$. When $1/\delta u = 0$ this model becomes equivalent to the BFM. We discretize time in units dt and space with periodic boundary conditions along x. To measure quasi-static avalanches, we apply a succession of kicks of sizes δw: we impose $\dot{u}_{tx} = m^2/\eta\delta w$ at $t = 0^+$ (beginning of the avalanche), iterate (14) and wait for the interface to stop before

applying a new kick [36]. To identify the seed of each avalanche, we record the velocity $v(x,t)$ for the $n_t = 10^3$ first time-steps of the avalanche. We find the position $x_{\max}(n_t)$ of maximum velocity at $t_{n_t} = n_t dt$ (or at the end of the avalanche if it has stopped before), and then successively identify at each time step $t_n < t_{n_t}$ the position $x_{\max}(n)$ defined as the neighbor of $x_{\max}(n+1)$ with the largest velocity at time t_n. $x_{\max}(n=1)$ is identified as the seed of the avalanche (see [36] for details).
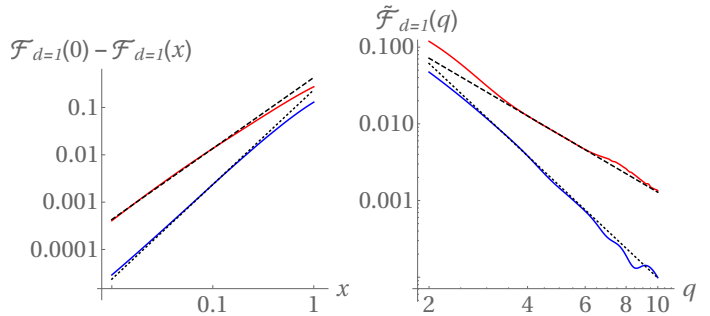

FIG. 5: Left: (resp. Right:) Log-Log plot of $\mathcal{F}_{d=1}(0) - \mathcal{F}_{d=1}(x)$ (resp. $\tilde{\mathcal{F}}_{d=1}(q)$) numerically obtained in the BFM model (blue) and in the SR model (red). Dotted lines: guide lines for the BFM result x^2 (left) and $1/q^4$ (right). Dashed lines: $x^{1.5}$ (left) and $1/q^{2.5}$ (right). These results are consistent with (i) the exact result $\tilde{\eta}_{d=1} = 4$ for the BFM (ii) $\tilde{\eta}_{d=1} \simeq 2.5$ for the SR model (in between the guess $\tilde{\eta}_{d=1}^{\mathrm{guess}} = d + \zeta \simeq 2.25$ and our $O(\epsilon)$ prediction $\tilde{\eta}_{d=1} \simeq 8/3 \simeq 2.66$).

In dimension $d=1$ we use a system of size $L = 2048$ discretized with $N = L$ points and a mass $m = 10/L$. In Fig. 4 we show our results for the mean-shape for different values of S and compare with our theoretical predictions using the predicted value of ℓ_σ (deduced from the measurement of S_m), hence with no fitting parameter. The results for the BFM are excellent. For the SR model, the improvement brought by the $O(\epsilon)$ correction is substantial. If one instead uses a measurement of ℓ_σ by e.g. setting the value of the shape at the origin, the agreement with the SR model is, to the naked eye, almost perfect. We also measure properties independent of the value of ℓ_σ: (i) in Fig.5 the small x and large q behaviors (ii) the universal ratios c_p. We obtain $(c_1, c_2) \simeq (1.699 \pm 0.003, 3.83 \pm 0.05)$ for the BFM and $(c_1, c_2) \simeq (1.612 \pm 0.004, 3.16 \pm 0.03)$ for the SR model (error-bars are 3 sigma estimates). The above predictions are in perfect agreement for the BFM, and our $O(\epsilon)$ corrections go in the right direction for the SR case.

To conclude, we introduced an original way of characterizing the mean shape of an avalanche by centering around its seed. We obtained theoretical predictions for this observable and confronted them to numerical simulations. We also proposed a protocol to measure it. We hope that this work stimulates measurements of this quantity in numerical setups and imaging experiments.

[1] J. P. Sethna, K. A. Dahmen, C. R. Myers, *Crackling Noise*, arXiv:cond-mat/0102091, Nature **410**, 242 (2001).

[2] J. Lin, E. Lerner, A. Rosso, M. Wyart, *Scaling description of the yielding transition in soft amorphous solids at zero temperature*, arXiv:1403.6735, PNAS **111** (40) 14382-14387 2014.

[3] M. Müller, M. Wyart, *Marginal Stability in Structural, Spin and Electron Glasses*, arXiv:1406.7669, Annu. Rev. Condens. Matter Phys. **6**, 9 (2015).

[4] K.M. Salerno, M.O. Robbins, *The effect of inertia on sheared disordered solids: Critical scaling of avalanches in two and three dimensions*,arXiv:1309.1872, Phys. Rev. E **88**, 062206 (2013).

[5] P. Dusan Ispanovity, L. Laurson, M. Zaiser, I. Groma, S. Zapperi, M. J. Alava, *Avalanches in 2D Dislocation Systems: Plastic Yielding is not Depinning*, arXiv:1307.3377, Phys. Rev. Lett. **112**, 235501(2014).

[6] D.S. Fisher, *Collective transport in random media: From superconductors to earthquakes*, Phys. Rep. **301** (1998) 113–150.

[7] G. Blatter, M.V. Feigelman, V.B. Geshkenbein, A.I. Larkin and V.M. Vinokur, *Vortices in high-temperature superconductors*, Rev. Mod. Phys., **66** (1994), 1125.

[8] T. Nattermann and S. Scheidl, *Vortex-glass phases in type-II superconductors*, Advances in Physics, **49** (2000), 607-704.

[9] T. Giamarchi and P. Le Doussal, *Statics and Dynamics of Disordered Elastic Systems*, arXiv:9705096, in A.P. Young, editor, *Spin glasses and random fields*, World Scientific, Singapore, 1997.

[10] S. Zapperi, P. Cizeau, G. Durin and H.E. Stanley, *Dynamics of a ferromagnetic domain wall: Avalanches, depinning transition, and the Barkhausen effect*, Phys. Rev. B **58** (1998) 6353–6366.

[11] G. Durin and S. Zapperi, *Scaling exponents for Barkhausen avalanches in polycrystalline and amorphous ferromagnets*, Phys. Rev. Lett. **84**, 4705-4708 (2000).

[12] S. Moulinet, C. Guthmann and E. Rolley, *Roughness and dynamics of a contact line of a viscous fluid on a disordered substrate*, Eur. Phys. J. E **8** (2002) 437443.

[13] P. Le Doussal, K.J. Wiese, S. Moulinet and E. Rolley, *Height fluctuations of a contact line: A direct measurement of the renormalized disorder correlator*, arXiv:0904.1123, EPL **87** (2009) 56001.

[14] Y. Ben-Zion and J. Rice, J. Geophys. Res. **98**, 14109 (1993), A. Mehta, K. Dahmen, and Y. Ben-Zion, arXiv:cond-mat/0509226, Phys. Rev. E **73**, 1 (2006), D. Fisher, K. Dahmen, S. Ramanathan, and Y. Ben-Zion, arXiv:cond- mat/9703029, Phys. Rev. Lett. **78**, 4885 (1997), Y. Ben-Zion and J. Rice, J. Geophys. Res. **102**, 17 (1997).

[15] L. Ponson *Depinning Transition in the Failure of Inhomogeneous Brittle Materials*, Phys. Rev. Lett. **103**, 055501 (2009).

[16] S. Santucci et al. *Fracture roughness scaling: A case study on planar cracks*, arXiv:1007.1188, EPL, **92** (2010) 44001

[17] D. Bonamy, S. Santucci and L. Ponson, *Crackling dynamics in material failure as the signature of a self-organized dynamic phase transition*, Phys. Rev. Lett. **101** (2008) 045501.

[18] L. Laurson, S. Santucci, S. Zapperi, *Avalanches and clusters in planar crack front propagation*, arXiv:0911.2380 Phys. Rev. E **81**, 046116 (2010).

[19] R. Planet, S. Santucci, and J. Ortín, *Avalanches and Non-Gaussian Fluctuations of the Global Velocity of Imbibition Fronts*, Phys. Rev. Lett. **102**, 094502 (2009) -

[20] S. Zapperi, C. Castellano, F. Colaiori, and G. Durin, *Signature of effective mass in crackling-noise asymmetry*, Nature Physics **1**, 46 (2005).

[21] S. Papanikolaou, F. Bohn, R.L. Sommer, G. Durin, S. Zapperi and J.P. Sethna, *Universality beyond power laws and the average avalanche shape*, Nature Physics **7** (2011) 316–320.

[22] L. Laurson, X. Illa, S. Santucci, K.T. Tallakstad, K.K Maloy and M.J. Alava *Evolution of the average avalanche shape with the universality class*, Nat. Commun. **4** (2013) 2927.

[23] A. Dobrinevski, P. Le Doussal, K.J. Wiese *Avalanche shape and exponents beyond mean-field theory*, EPL **108** (2014) 66002.

[24] B. Alessandro, C. Beatrice, G. Bertotti and A. Montorsi, *Domain-wall dynamics and Barkhausen effect in metallic ferromagnetic materials. I. Theory*, Journal of Applied Physics **68** (1990) 2901.

[25] B. Alessandro, C. Beatrice, G. Bertotti and A. Montorsi, *Domain-wall dynamics and Barkhausen effect in metallic ferromagnetic materials. II. Experiments*, Journal of Applied Physics **68** (1990) 2908.

[26] P. Le Doussal and K.J. Wiese, *First-principle derivation of static avalanche-size distribution*, Phys. Rev. E **85** (2011) 061102, arXiv:1111.3172.

[27] T. Thiery, P. Le Doussal and K.J. Wiese, *Spatial shape of avalanches in the Brownian force model*, arXiv:1504.05342, Journal of Statistical Mechanics: Theory and Experiment, **8**, P08019 (2015).

[28] A. Dobrinevski, P. Le Doussal and K.J. Wiese, *Nonstationary dynamics of the Alessandro-Beatrice-Bertotti-Montorsi model*, Phys. Rev. E **85** (2012) 031105, arXiv:1112.6307.

[29] P. Le Doussal and K.J. Wiese, *Avalanche dynamics of elastic interfaces*, Phys. Rev. E **88** (2013) 022106, arXiv:**1302.4316**.

[30] D.S. Fisher, Phys. Rev. Lett. **56** (1986) 1964.

[31] T. Nattermann, et al., J. Phys. II (France) **2** (1992) 1483.

[32] O. Narayan and D.S. Fisher, Phys. Rev. B **46** (1992) 11520; Phys. Rev. B **48** (1993) 7030.

[33] P. Chauve, P. Le Doussal and K.J. Wiese, Phys. Rev. Lett. **86** (2001) 1785, P. Le Doussal, K.J. Wiese and P. Chauve, Phys. Rev. E **69** (2004) 026112; Phys. Rev. B **66** (2002) 174201.

[34] K. Dahmen and J.P. Sethna, *Hysteresis, avalanches, and disorder-induced critical scaling: A renormalization-group approach*, Phys. Rev. B **53** (1996) 14872–14905.

[35] P. Le Doussal and K.J. Wiese, *Size distributions of shocks and static avalanches from the functional renormalization group*, Phys. Rev. E **79** (2009) 051106, arXiv:0812.1893.

[36] see Supplemental Materials.

[37] A. Dobrinevski, P. Le Doussal, K. Wiese, in preparation

[38] P. Le Doussal and K.J. Wiese, *Distribution of velocities in an avalanche*, EPL **97** (2012) 46004, arXiv:**1104.2629**.

[39] A. Dobrinevski, *Field theory of disordered systems*

- *Avalanches of an elastic interface in a random medium*, PhD thesis, Ecole Normale Supérieure (2013), arXiv:1312.7156.

[40] P. Le Doussal and K.J. Wiese, *An exact mapping of the stochastic field theory for Manna sandpiles to interfaces in random media*, arXiv:1410.1930, Phys. Rev. Lett. **114**, 110601 (2014).

[41] P. Martin, E. Siggia, and H. Rose, *Statistical Dynamics of Classical Systems*, Phys. Rev. A **8**, 423-437 (1973).

[42] H.K. Janssen, *On a Lagrangean for classical field dynamics and renormalization group calculations of dynamical critical properties*, Z. Phys. B **23** (1976), 377-380.

[43] M. Delorme, P. Le Doussal and K.J. Wiese, in prepara-tion.

[44] A. Rosso, A. Hartmann, and W. Krauth, *Depinning of elastic manifolds*, Phys. Rev. E, **67**(2):021602, February 2003.

[45] E. E. Ferrero, S. Bustingorry, and A. B. Kolton, *Non-steady relaxation and critical exponents at the depinning transition,* Phys. Rev. E, **87**(3):032122, March 2013.

[46] I. Dornic, H. Chaté and M.A. Munoz, *Integration of Langevin Equations with Multiplicative Noise and the Viability of Field Theories for Absorbing Phase Transitions*, Phys. Rev. Lett. **94**, (2005) 100601.

Supplemental Material

We give here a derivation of the results presented in the main text and details on the numerical simulations.

Dynamical Field Theory Setting

Equation of motion and dynamical action

As written in the main text, we consider the equation of motion for the over-damped dynamic of an elastic interface of internal dimension d in a quenched random force field and driven by a parabolic well of position w_{xt}

$$\eta \partial_t u_{xt} = \nabla_x^2 u_{xt} - m^2(u_{xt} - w_{xt}) + F(u_{xt}, x) \tag{15}$$

where $x \in \mathbb{R}^d$, $t \in \mathbb{R}$, $u_{xt} \in \mathbb{R}$ (the space-time dependence is indicated by subscripts). The elastic-coefficient as been set to unity by a choice of units. In this formulation, the driving force of the parabolic well is $f_{xt} = m^2(w_{xt} - u_{xt})$. The pinning force $F(u, x)$ is chosen centered, Gaussian with second cumulant $\overline{F(u, x)F(u', x')} = \delta^d(x - x')\Delta_0(u - u')$ (the overline denotes the average over disorder) where $\Delta_0(u)$ is a short-ranged function. Higher cumulant can also exist (i.e. non Gaussian force, and are taken into account in the FRG treatment). Note that here we have written the case of short-ranged (SR) elasticity with an elastic term of the form $\nabla_x^2 u_{xt}$. Other elastic kernels can also be considered, by changing

$$\nabla_x^2 u_{xt} - m^2 u_{xt} \rightarrow \int_{x'} g_{xx'}^{-1} u_{x't} \tag{16}$$

where $g_{xx'}^{-1}$ is a translationally invariant ($g_{xx'}^{-1} = g_{x-x'}^{-1}$) elastic kernel. In particular, we will consider the following kernel (here written in Fourier space) ($g_q^{-1} = \int_x e^{iqx} g_x^{-1}$, here and throughout the rest of the Supplemental Material $\int_x = \int_{x \in \mathbb{R}^d} d^d x$ and $\int_q = \int_{q \in \mathbb{R}^d} \frac{d^d q}{(2\pi)^d}$)

$$g_q^{-1} = \sqrt{\mu^2 + q^2} \tag{17}$$

which is known to be relevant in the description of standard long-ranged (LR) elasticity. In this situation, the parameter μ is related to the mass m as $m = \sqrt{\mu}$. In most of the following, we will deal with the SR elasticity case, and explicitly mention when we consider the LR one. Introducing a response field $\tilde{u}_{xt}$, the generating function of the velocity field $G[\lambda_{xt}] = \overline{e^{\int_{xt} \lambda_{xt} \dot{u}_{xt}}}$ is computed using the dynamical action formalism [41, 42]:

$$G[\lambda_{xt}] = \int D[\tilde{u}]D[\dot{u}] e^{\int_{xt} \lambda_{xt} \dot{u}_{xt} + m^2 \int_{xt} \tilde{u}_{xt} \dot{w}_{xt} - S_0 - S_{dis}}$$

$$S_0 = \int_{xt} \tilde{u}_{xt}(\eta \partial_t - \nabla^2 + m^2)\dot{u}_{xt} \quad , \quad S_{dis} = -\frac{1}{2}\int_{xtt'} \tilde{u}_{xt}\tilde{u}_{xt'} \partial_t \partial_{t'} \Delta_0(u_{xt} - u_{xt'}) \tag{18}$$

The renormalized field theory

As discussed in [29], in the limit of small m, and in the quasi-static limit $\dot{w}_{xt} = v \rightarrow 0^+$, universal quantities associated to the motion inside a single avalanche can be computed in an expansion in $\epsilon = 4 - d$ using an effective action identical to (18) with the replacement $\Delta_0(u) \rightarrow \Delta(u) = \Delta(0) - \sigma|u| - 4\pi^2 \alpha m^{4-d} u^2 + O(\epsilon^2)$, where σ and

$\alpha = O(\epsilon)$ are renormalized quantities. σ is a non-universal parameter whose value is related to the two first moments of the avalanche size distribution through the exact relation $2\sigma/m^4 = \langle S^2 \rangle / \langle S \rangle$. On the other hand α is dimensionless and universal at the FRG fixed point with value $\alpha = -2\epsilon/9 + O(\epsilon^2)$. In terms of the action, this replacement reads $S_{dis} \to S_{dis}^{eff} = S_{tree} + \delta_{1-loop}S$ with

$$S_{tree} = -\sigma \int_{xt} \tilde{u}_{xt}^2 \dot{u}_{xt} \quad , \quad \delta_{1-loop}S = -4\pi^2\alpha m^{4-d} \int_{xtt'} \tilde{u}_{xt} \dot{u}_{xt} \tilde{u}_{xt'} \dot{u}_{xt'} \tag{19}$$

At lowest order in ϵ, the action is $S_{dis}^{eff} = S_{tree}$. Using the renormalized value of σ, it gives the exact result for universal quantities in $d > 4$. In any dimension, this tree/mean-field theory also corresponds to an interface slowly driven in a Brownian force landscape: for each x, $F(u,x)$ is a Brownian in u independent of the others with $\overline{(F(u',x) - F(u,x))^2} = 2\sigma|u' - u|$. This is the Brownian Force Model (BFM). The $O(\epsilon)$ corrections around the BFM are easily computed using the fact that $\delta_{1-loop}S$ can also be taken into account by introducing a fictitious Gaussian centered white noise ξ_{xt} with correlations $\langle \xi_x \xi_{x'} \rangle_\xi = 8\pi^2\alpha m^{4-d}\delta^d(x - x')$ through the identity

$$e^{-S_0 - S_{dis}^{eff}} = \langle e^{-\int_{xt} \tilde{u}_{xt}(\eta\partial_t - \nabla^2 + m^2 + \xi_x)\dot{u}_{xt} - S_{tree}} \rangle_\xi \tag{20}$$

where $\langle \rangle_\xi$ denotes the average over ξ. One-loop observables are thus rewritten as averaged tree observables in a theory with space-dependent mass $m^2 \to m^2 + \xi_x$. Since $\xi_x = O(\sqrt{\epsilon})$, the effect of ξ_x can be taken into account pertubatively up to order $O(\xi_x^2)$.

Avalanches observables

Avalanches in non-stationary driving

Let us first introduce our avalanche observables in a non-stationary setting. We refer the reader to [27–29] for more details on this procedure. We first prepare the interface is in its quasi-static stationary state $\dot{w}_{xt} \sim v = 0^+$, then turn the driving off: $\dot{w}_{xt} = 0$ and finally wait for the interface to stop at some metastable position. Supposing we are in such a state at $t = 0$, we apply to the interface a step in the driving force localized at $x = t = 0$, $\dot{f}_{xt} = m^2\delta w\delta(x)\delta(t)$ (local kick) and let it evolve. Information about the resulting motion of the interface is encoded in the generating functional $G[\lambda_{xt}] = \overline{e^{\int_{x,t>0} \lambda_{xt}\dot{u}_{xt}}}$. Remarkably, since the action (19) (written at one-loop in terms of ξ_x (20)) is linear in $\dot{u}_{xt}$, the evaluation of $G[\lambda_{xt}]$ through the path-integral formalism simplifies. The integration on the velocity field $\dot{u}_{xt}$ leads to a delta functional and to the result:

$$G[\lambda_{xt}] = \langle e^{m^2\delta w \tilde{u}_{x=t=0}^{\lambda,\xi}} \rangle_\xi \tag{21}$$

where $\tilde{u}_{xt}^{\lambda,\xi}$ is the solution of the so-called instanton equation:

$$\partial_t \tilde{u}_{xt} + \nabla^2 \tilde{u}_{xt} - (1 + \xi_x)\tilde{u}_{xt} + \tilde{u}_{xt}^2 + \lambda_{xt} = 0 \tag{22}$$

here written in dimensionless units using the variables $\tilde{u}_x = \frac{m^2}{\sigma}\hat{\tilde{u}}_{\hat{x}}$, $x = \hat{x}/m$, $t = \frac{\eta}{m^2}\hat{t}$, $\lambda_{xt} = \frac{m^4}{\sigma}\hat{\lambda}_{\hat{x}\hat{t}}$, and omitting the hats in what follows, to lighten notations. The boundary conditions is $\tilde{u}_{xt} = 0$ for $t = +\infty$. Here we will only be interested in single avalanche, defined as the response of the interface to an infinitesimal step in the force. We introduce the generating functional $Z[\lambda_{xt}]$ as

$$\overline{e^{\int_{x,t>0} \lambda_{xt}\dot{u}_{xt}} - 1} = \delta w Z[\lambda_{xt}] + O(\delta w^2)$$
$$Z[\lambda_{xt}] = m^2 \langle \tilde{u}_{x=t=0}^{\lambda,\xi} \rangle_\xi \tag{23}$$

In the above expansion, the δw factor just accounts for the probability to trigger an avalanche at $t = x = 0$. Introducing $\rho_{t=x=0}[\dot{u}_{xt}]$, the density of velocity field $\dot{u}_{tx}$ inside an avalanche that starts at $t = x = 0$, we write

$$Z[\lambda_{xt}] = \int D[\dot{u}] \left(e^{\int_{xt} \lambda_{xt}\dot{u}_{xt}} - 1 \right) \rho_{t=x=0}[\dot{u}_{xt}]. \tag{24}$$

The fact that these definitions indeed correspond to what is usually meant by avalanches in the quasi-static limit is discussed below. This formulation is up to now completely general. Let us now focus on two types of sources: $\lambda_{xt}^1 = (-\mu + \lambda\delta(x - y)\delta(t - s))\theta(t)$ and $\lambda_{xt}^2 = (-\mu + \lambda\delta(x - y))\theta(t)$ ($\theta(.)$ denotes the Heaviside theta function). In both cases, the μ variable probes the total size of the avalanche $S = \int_{x,t>0} \dot{u}_{xt}$. In the first case, λ probes the local velocity at $t = s$ and $x = y$ during the avalanche. In the second case, λ probes the local size of the avalanche at $x = y$,

$S_y = \int_{t>0} \dot{u}_{yt}$. We write the associated generating function $Z^{(1)}[\lambda_{xt}^1] = Z^{(1)}(\mu, \lambda, y, s)$ and $Z^{(2)}[\lambda_{xt}^2] = Z^{(2)}(\mu, \lambda, y)$. These are obtained through the formula (23) by solving (22) which leads to

$$Z^{(1)}(\mu, \lambda, y, s) = \int dS d\dot{u}_{ys} e^{-\mu S + \lambda \dot{u}_{ys}} \rho_{t=x=0}^{(1)}(S, \dot{u}_{ys}) \quad , \quad Z^{(2)}(\mu, \lambda, y) = \int dS dS_y e^{-\mu S + \lambda S_y} \rho_{t=x=0}^{(2)}(S, S_y), \quad (25)$$

where $\rho_{t=x=0}^{(1)}(S, \dot{u}_{ys})$ (resp. $\rho_{t=x=0}^{(2)}(S, \dot{u}_{ys})$) is the joint density of total size S and velocity field $\dot{u}_{ys}$ (resp. of total size S and local size S_y) for avalanches starting at $t = x = 0$. In practice we will only be interested in computing the mean velocity-field inside avalanche of total size S, $\langle \dot{u}_{ys} \rangle_S$ (resp. the mean local size inside avalanche of total size S, $\langle S_y \rangle_S$). These are computed as

$$\langle \dot{u}_{ys} \rangle_S = \frac{LT_{\mu \to S}^{-1} \partial_\lambda Z^{(1)}|_{\lambda=0}}{\rho(S)/L^d} \quad , \quad \langle S_y \rangle_S = \frac{LT_{\mu \to S}^{-1} \partial_\lambda Z^{(2)}|_{\lambda=0}}{\rho(S)/L^d} = \int_{s=0}^{\infty} ds \langle \dot{u}_{ys} \rangle_S \quad (26)$$

where $LT_{\mu \to S}^{-1}$ denotes the Inverse Laplace Transform (ILT) operation $LT_{\mu \to S}^{-1} = \frac{1}{2i\pi} \int_{\mathcal{C}} d\mu e^{\mu S}$ with appropriate contour of integration, and we have introduced $\rho(S)$ the density of avalanches of total size S, previously computed up to one-loop in [26, 29, 35] ($\rho(S)/L^d = \int d\dot{u}_{ys} \rho_{t=x=0}^{(1)}(S, \dot{u}_{ys}) = \int dS_y \rho_{t=x=0}^{(2)}(S, S_y)$ is the density of avalanches of total size S starting at $x = 0$). For the observables we are interested in, we will thus only need to solve (22) at first order in λ.

Link with the stationary driving

Let us now present here how the precedent approach is linked to avalanches occurring in the quasi-static stationary state of the interface dynamic $\dot{w}_{xt} = v \to 0^+$. We introduce ρ_0 the mean density of avalanche per unit of driving and $p[\dot{u}_{tx}]$ the (functional) probability of velocity field $\dot{u}_{tx}$ inside an avalanche. At first order in v, the generating function $G[\lambda_{xt}] = \overline{e^{\int_{xt} \lambda_{xt} \dot{u}_{xt}}}$ can be written as

$$G[\lambda_{xt}] = (1 - \rho_0 vT) + \rho_0 vT \int D[\dot{u}] e^{\int_{xt} \lambda_{xt} \dot{u}_{xt}} p[\dot{u}_{xt}] + O(v^2) = 1 + vT \int D[\dot{u}] \left(e^{\int_{xt} \lambda_{xt} \dot{u}_{xt}} - 1 \right) \rho[\dot{u}_{xt}] + O(v^2) \quad (27)$$

where we reintroduced $\rho[\dot{u}_{xt}] = \rho_0 p[\dot{u}_{tx}]$ the density of velocity field $\dot{u}_{tx}$ inside an avalanche. The equation (27) can be seen as a definition of what is meant by avalanches in the quasi-static setting. The time scale T that appears in (27) should be much larger than the time-scale of avalanche motion (to allow the avalanche to terminate) and much smaller than the typical waiting time between avalanches. This only works if λ_{xt} is also non-zero in a time window smaller than T: this ensures that the measurement made on the velocity-field is also inside a single-avalanche. On the other hand, the small velocity expansion made directly on the action (18) and compared to (27) gives

$$G[\lambda_{xt}] = 1 + v \langle m^2 \int_{xt} \tilde{u}_{xt} \rangle_{\lambda_{xt}} \longrightarrow \int D[\dot{u}] \left(e^{\int_{xt} \lambda_{xt} \dot{u}_{xt}} - 1 \right) \rho[\dot{u}_{xt}] = \int_{xt} \frac{m^2}{T} \langle \tilde{u}_{xt} \rangle_{\lambda_{xt}} \quad (28)$$

In the right of (28), the integral over time and space originates from the fact that we have consider the effect of avalanches starting at any point of the interface, and at any time in the time-window T. From a field-theory point of view, it is then natural to interpret $m^2 \langle \tilde{u}_{x=t=0} \rangle_{\lambda_{xt}}$ as the contribution from avalanches starting at $t = x = 0$ (diagrams entering into $\langle \tilde{u}_{x=t=0} \rangle_{\lambda_{xt}}$ can only have a first non-zero $\dot{u}_{xt}$ at $x = 0$). Furthermore, this is supported by the non-stationary setting in which this interpretation is immediate. In the quasi-static setting we can only a priori consider sources λ_{xt} non-zero in time windows smaller than T to make sure that only one avalanche is taken into account. However, from a practical point of view, when $T >> \tau_m$ where τ_m is the typical time scale of avalanches, both descriptions give exactly the same result as detailed in [29, 37].

Calculation in the BFM

Mean-velocity field inside an avalanche in the BFM

Here we give the calculation for the mean-velocity field inside avalanche of total size S in the BFM $\langle \dot{u}_{ys} \rangle_S$ (denoted $v(y, s)$ in the main text with $y = x$ and $s = t$). We have to solve to first order in λ the instanton equation

$$\partial_t \tilde{u}_{xt} + \nabla^2 \tilde{u}_{xt} - \tilde{u}_{xt} + \tilde{u}_{xt}^2 - \mu + \lambda \delta(x - y) \delta(t - s) = 0 \ . \quad (29)$$

Note that here, in dimensionless units, time and avalanche size are measured in terms of the natural units of avalanches motion $\tau_m = \eta/m^2$ and $S_m = \sigma/m^4$. The perturbative solution is $\tilde{u}_{xt} = \tilde{u}_{xt}^0 + \tilde{u}_{xt}^1 \lambda + O(\lambda^2)$ with

$$\tilde{u}_x^0 = Z(\mu) = \frac{1}{2} \left(1 - \kappa^2(\mu) \right) \quad , \quad \kappa(\mu) = (1 + 4\mu)^{\frac{1}{4}} \quad , \quad \tilde{u}_{qt}^1 = -\int_{t'=+\infty}^{t} e^{(q^2 + \kappa^2(\mu))(t-t') + iqy} \delta(t' - s) dt' \quad (30)$$

here written in Fourier space for the $O(\lambda)$ part: $\tilde{u}^1_{qt} = \int_x e^{iqx} \tilde{u}^1_{xt}$. This immediately gives

$$\tilde{u}^1_{t=x=0} = \int_q e^{iqy-(q^2+\kappa^2(\mu))s} \tag{31}$$

Using the tree result for the avalanche size density $\rho^{\mathrm{MF}}(S) = \frac{L^d}{2\sqrt{\pi}S^{3/2}}e^{-S/4}$ we obtain the mean velocity field inside a single avalanche using (26) as

$$< \dot{u}_{ys} >_S = 2\sqrt{\pi}S^{3/2}e^{S/4}LT^{-1}_{\mu\to S}\int_q e^{iqy-(q^2+\sqrt{1+4\mu})s} = 2se^{-\frac{s^2}{S}}\int_q e^{iqy-q^2s} = 2se^{-s^2/S}\frac{1}{(4\pi s)^{d/2}}e^{-y^2/(4s)} \tag{32}$$

In the notation of the main text, we thus obtain (4) that we recall here

$$< v(x,t) >_S = S^{\frac{2-d}{4}}F(t/S^{1/2}, x/S^{1/4}) \quad , \quad F(t,x) = 2te^{-t^2}\frac{1}{(4\pi t)^{d/2}}e^{-x^2/(4t)} \tag{33}$$

Extension to LR elasticity

Following the same computation, one obtains for the case of the BFM with long-ranged elasticity (with the kernel (17))

$$\tilde{u}_{t=x=0} = \int_q e^{iqy-(\sqrt{1+q^2}-1+\kappa^2(\mu))s} \tag{34}$$

And thus

$$< \dot{u}_{ys} >_S = 2se^{-\frac{s^2}{S}}\int_q e^{iqy-(\sqrt{1+q^2}-1)s} \tag{35}$$

Note that here, the spatio-temporal shape does not satisfy the expected scaling form (2), $< \dot{u}_{ys} >_S = S^{\frac{2-d-1}{2}}F(s/S^{\frac{1}{2}}, y/S^{\frac{1}{2}})$ for all S. This should not be surprising, it is known that the present theory describes scale-invariant avalanches only for $S \ll S_m$ (here $S_m = 1$ in dimensionless units). The fact that the scaling hypothesis for the mean velocity field holds $\forall S$ in the BFM with short-ranged elasticity is the true surprise. Scaling in the long-ranged model is restored at small S and here

$$F(s,y) = \lim_{S\to 0}S^{\frac{d-1}{2}}< \dot{u}_{S^{\frac{1}{2}}y,S^{\frac{1}{2}}s} >_S = 2se^{-s^2}\int_q e^{iqy-|q|s} \tag{36}$$

Evaluating this integral in dimension 1 immediately leads to the result (7).

The mean shape of avalanches in the BFM: results in Fourier space

Using (31), we immediately obtain the mean-shape of avalanche in Fourier space in the BFM as

$$\tilde{\mathcal{F}}^{\mathrm{MF}}(q) = \int_{s=0}^{\infty}2se^{-s^2-q^2s} = 1 - \frac{\sqrt{\pi}q^2}{2}e^{\frac{q^4}{4}}\mathrm{erfc}\left(\frac{q^2}{2}\right) \tag{37}$$

i.e. the result (5) of the main text. Note that here avalanche sizes have been expressed in units of $S_m = \sigma/m^4$ and distances in units of $1/m$. Hence the non-universal scale ℓ_σ of the main text is indeed $\ell_\sigma = \frac{1}{m}S_m^{-1/4} = \sigma^{-1/4}$. Let us give here the large and small momenta behavior of $\tilde{\mathcal{F}}^{\mathrm{MF}}(q)$:

$$\tilde{\mathcal{F}}^{\mathrm{MF}}(q) =_{q\gg 1} \frac{2}{q^4} - \frac{12}{q^8} + \frac{120}{q^{12}} + O(\frac{1}{q^{16}}) \tag{38}$$

$$\tilde{\mathcal{F}}^{\mathrm{MF}}(q) =_{q\ll 1} 1 - \frac{\sqrt{\pi}q^2}{2} + \frac{q^4}{2} - \frac{\sqrt{\pi}q^6}{8} + O\left(q^8\right) \tag{39}$$

Extension to LR elasticity

The extension of the precedent results to the case of LR elasticity is straightforward. As written in the main text and following the formula (36), the mean-shape in Fourier space in the scaling regime for LR elasticity is simply obtained from the precedent results by changing $q^2 \to q$:

$$\tilde{\mathcal{F}}^{\mathrm{MF,LR}}(q) = \tilde{\mathcal{F}}^{\mathrm{MF}}(\sqrt{q}). \tag{40}$$

In particular it now has an algebraic tail at large q with exponent $1/q^2$, $\tilde{\mathcal{F}}^{\mathrm{MF,LR}}(q) \simeq_{q \gg 1} \frac{2}{q^2}$.

The mean shape of avalanches in the BFM: results in real space

In real space, $\mathcal{F}_d^{\mathrm{MF}}(x)$ is most simply obtained by integration of (33):

$$\mathcal{F}_d^{\mathrm{MF}}(x) = \frac{2}{(4\pi)^{d/2}} \int_0^{+\infty} dt\, t^{1-d/2} e^{-t^2 - \frac{x^2}{4t}} \tag{41}$$

This integral can be expressed either as the sum of three series:

$$\mathcal{F}_d^{\mathrm{MF}}(x) = \pi^{1-\frac{d}{2}} \sum_{p=0}^{\infty} (-1)^p 2^{-4p} \big[\frac{a_p}{\sin \frac{d\pi}{4}} x^{4p} - \frac{a_{p+\frac{1}{2}}}{4 \cos \frac{d\pi}{4}} x^{4p+2} + \frac{b_p}{\sin \frac{d\pi}{2}} x^{4-d+4p} \big] \tag{42}$$

$$a_p = \frac{2^{-d}}{(2p)! \Gamma\left(\frac{d}{4}+p\right)} \quad , \quad b_p = \frac{2^{-3}}{p! \Gamma\left(-\frac{d}{2}+2p+3\right)} \tag{43}$$

or, equivalently, as the sum of three generalized hypergeometric functions (corresponding term by term to the series):

$$\mathcal{F}_d^{\mathrm{MF}}(x) = \frac{1}{8} \pi^{1-\frac{d}{2}} \left(\frac{2^{3-d} \csc\left(\frac{\pi d}{4}\right) {}_0F_2\left(; \frac{1}{2}, \frac{d}{4}; -\frac{x^4}{64}\right)}{\Gamma\left(\frac{d}{4}\right)} - \frac{2^{1-d} x^2 \sec\left(\frac{\pi d}{4}\right) {}_0F_2\left(; \frac{3}{2}, \frac{d}{4}+\frac{1}{2}; -\frac{x^4}{64}\right)}{\Gamma\left(\frac{d+2}{4}\right)} \right.$$

$$\left. + \frac{x^{4-d} \csc\left(\frac{\pi d}{2}\right) {}_0F_2\left(; \frac{3}{2}-\frac{d}{4}, 2-\frac{d}{4}; -\frac{x^4}{64}\right)}{\Gamma\left(3-\frac{d}{2}\right)} \right) \tag{44}$$

The expressions (42) and (44) are adequate for $d = 1, 3$. For $d = 2, 4$ one must first take the limit $d \to 2, 4$ before evaluating. This is easy to do with mathematica, and we give here only the two leading terms at small x:

$$\mathcal{F}_2^{\mathrm{MF}}(x) = \frac{1}{4\sqrt{\pi}} - \frac{x^2(-4\log(x) - 3\gamma_E + 2 + \log(16))}{16\pi} + O\left(x^3\right) \tag{45}$$

$$\mathcal{F}_4^{\mathrm{MF}}(x) = \frac{-4\log(x) - 3\gamma_E + \log(16)}{16\pi^2} + \frac{x^2}{32\pi^{3/2}} + O\left(x^3\right) \tag{46}$$

For $d < 4$ the value at zero is finite:

$$\mathcal{F}_d^{\mathrm{MF}}(0) = \frac{2^{-d} \pi^{1-\frac{d}{2}}}{\Gamma\left(\frac{d}{4}\right) \sin\left(\frac{\pi d}{4}\right)} \tag{47}$$

$$\mathcal{F}_1^{\mathrm{MF}}(0) \approx 0.345684 \quad , \quad \mathcal{F}_2^{\mathrm{MF}}(0) \approx 0.141047 \quad , \quad \mathcal{F}_4^{\mathrm{MF}}(0) \approx 0.0813891 \tag{48}$$

and $\mathcal{F}_d^{\mathrm{MF}}(0)$ diverges as $\frac{1}{4\pi^2\epsilon}$ as $d \to 4^-$ (it has a minimum near $d = 3.2$). For $d > 4$ it diverges near zero as $\mathcal{F}_1^{\mathrm{MF}}(x) \simeq \frac{\pi^{1-\frac{d}{2}} \csc\left(\frac{\pi d}{2}\right)}{8\Gamma\left(3-\frac{d}{2}\right)} x^{4-d}$. The large distance behavior is easily obtained from the saddle-point method on (41). It yields a stretched exponential decay at large x with exponent $4/3$, independent of d:

$$\mathcal{F}_d^{\mathrm{MF}}(x) \simeq \frac{2^{-d/2} \pi^{\frac{1}{2}-\frac{d}{2}}}{\sqrt{3}} x^{\frac{2-d}{3}} e^{-\frac{3x^{4/3}}{4}} \tag{49}$$

Extension to LR elasticity

We did not attempt to find expressions for the mean-shape in real space for LR elasticity in any d. In the most experimentally relevant case of $d = 1$ however it takes a simple expression: integrating (7) from $t = 0$ to $t = \infty$ leads

$$\mathcal{F}_{d=1}^{\mathrm{MF,LR}}(x) = \frac{1}{\sqrt{\pi}} - x e^{x^2} \mathrm{erfc}(x) . \tag{50}$$

We note in particular the behavior around $x = 0$, $\mathcal{F}_{d=1}^{\mathrm{MF,LR}}(x) =_{x \ll 1} \frac{1}{\sqrt{\pi}} - |x| + O(x^2)$, reminiscent of the $2/q^2$ tail in Fourier space. At large x, the mean-shape now decays algebraically as $\mathcal{F}_{d=1}^{\mathrm{MF,LR}}(x) =_{x \gg 1} \frac{1}{2\sqrt{\pi}x^2} + O(1/x^4)$.

$O(\epsilon)$ corrections

"Brut" corrections

At $O(\epsilon)$ we focus directly on the computation of the mean-shape at fixed size $\langle S_y \rangle_S$. We need to solve

$$\partial_t \tilde{u}_{xt} + \nabla^2 \tilde{u}_{xt} - (1 + \xi_x)\tilde{u}_{xt} + \tilde{u}_{xt}^2 - \mu + \lambda\delta(x - y) = 0 \ . \tag{51}$$

at order 1 in λ and order 2 in ξ_x. We can look for time-independent solution and use a double expansion $\tilde{u}_x = \sum_{i=0}^{1}\sum_{j=0}^{2} \tilde{u}_j^i(x)$ where $\tilde{u}_j^i(x) = O(\lambda^i \xi^j)$. The observable of interest is $\mathcal{Z}(\mu, y) = \partial_\lambda Z^{(2)}(\mu, y, \lambda)|_{\lambda=0}$ where $Z^{(2)}$ was introduced in (23). Using $Z^{(2)}(\mu, y, \lambda) = m^2 \langle \tilde{u}_{x=0} \rangle_\xi$ we obtain (in dimensionless units)

$$\mathcal{Z}(\mu, y) = \mathcal{Z}^{\mathrm{MF}}(\mu, y) + \delta\mathcal{Z}(\mu, y) \quad , \quad \mathcal{Z}^{\mathrm{MF}}(\mu, y) = \tilde{u}_0^1(x = 0) \quad , \quad \delta\mathcal{Z}(\mu, y) = \langle \tilde{u}_2^1(x = 0) \rangle_\xi \tag{52}$$

These are most simply expressed in Fourier space $\tilde{\mathcal{Z}}(\mu, q) = \int_x e^{iqy}\mathcal{Z}(\mu, y)$ and we find

$$\tilde{\mathcal{Z}}^{\mathrm{MF}}(\mu, q) = G_q(\mu) = \frac{1}{q^2 + \kappa^2(\mu)}$$

$$\delta\tilde{\mathcal{Z}}(\mu, q) = 8\pi^2\alpha(G_q(\mu))^2 \left(\int_p G_p(\mu)\left(1 + 2Z(\mu)G_{p-q}(\mu)\right)^2 + 2G_0(\mu)\int_p \left(1 + Z(\mu)G_p(\mu)\right)Z(\mu)G_p(\mu) \right) \tag{53}$$

where we have introduced the response function $G_q(\mu)$, a dressed version of the elastic kernel $g_q = \frac{1}{m^2+q^2}$.

Counter-terms

The result for $\delta\tilde{Z}(\mu, q)$ is not yet complete: the integrals present in (53) diverge at large q for $d < 4$. This is a usual feature of one-loop computations in field theory. As detailed in [29], when doing a pertubative calculation in (19), one has to take into account a renormalization of σ and m^2 (the latter being in fact an artifact due to the utilization of the oversimplified one-loop action (19)). For clarity let us now denotes σ_0 and m_0^2 the parameters used so far in the perturbative calculation. These are renormalized as $\sigma_0 \to \sigma = \sigma_0 + \delta\sigma$ and $m_0^2 \to m^2 = m_0^2 + \delta m^2$ with

$$\delta\sigma = 24\pi^2\alpha \int_k g_k^2 \quad , \quad \delta m^2 = -8\pi^2\alpha \int_k g_k \tag{54}$$

where $g_k = \frac{1}{k^2+m_0^2}$ is the bare propagator. The parameters entering in (54) are either the bare parameters or the renormalized parameters (these choices differ from a term of order $O(\epsilon^2)$). The fact that the theory is renormalizable imply that divergences present in (53) should disappear when expressing the results in terms of renormalized parameters. Let us thus denote $\{K_0\} := \{\sigma_0, m_0^2\}$ the set of important couplings and emphasize the dependance of $\tilde{\mathcal{Z}}(\mu, q)$ by momentarily adopting the simple notation $\tilde{\mathcal{Z}}(\{K_0\})$. Rewriting the result $\tilde{\mathcal{Z}}(\{K_0\})$ in terms of the renormalized coupling $\{K\}$ leads to the definition of the counter-terms $\delta_{c.t.}\tilde{Z}(\{K\})$ as

$$\tilde{\mathcal{Z}}(\{K_0\}) = \tilde{\mathcal{Z}}(\{K - \delta K\}) = \tilde{\mathcal{Z}}^{\mathrm{MF}}(\{K\}) + \delta_{c.t.}\tilde{\mathcal{Z}}(\{K\}) + \delta\tilde{\mathcal{Z}}(\{K\}) + O(\epsilon^2) \tag{55}$$

and thus $\delta_{c.t.}\tilde{\mathcal{Z}}(\{K\}) = -\frac{\partial\tilde{\mathcal{Z}}^{\mathrm{MF}}(\{K\})}{\partial K_\alpha}\delta K_\alpha$. To compute these partial derivatives, we reintroduce the original units of the problem in $\tilde{\mathcal{Z}}^{\mathrm{MF}}(\{K\})$:

$$\tilde{\mathcal{Z}}^{\mathrm{MF}}(\{K\}) = \frac{e^{iqy}}{q^2 + \sqrt{1 + 4\sigma\mu/m^4}} \tag{56}$$

The $\frac{m^2}{\sigma}$ comes from the rescaling of $\tilde{u}$, the m^{-d} from the rescaling of the Fourier Transform and the $\frac{\sigma}{m^{4-d}}$ from the rescaling of λ. Computing the derivatives with respect to σ and m^2 and going back to dimensionless units leads to the following expression for the counter terms:

$$\delta_{c.t.}\tilde{\mathcal{Z}}(\mu, q) = 8\pi^2\alpha e^{iqy}G_{q=0}(\mu)G_q(\mu)^2(6\mu\int_k g_k^2 - \int_k g_k) \tag{57}$$

It is then easy to check that adding (57) to (53) indeed regularizes the result. The computation of the resulting, convergent integrals in $d = 4$ leads to the full result for the one loop correction $\delta\tilde{Z}(\mu, q) \to \delta\tilde{Z}(\mu, q) + \delta_{c.t.}\tilde{Z}(\mu, q)$ with

$$\delta\tilde{\mathcal{Z}}(\mu,q) = \alpha(G_q(\mu))^2 \left(\frac{(1+6\mu)\log(1-2Z)+2Z}{2(1-2Z)} + 4Z\left(1 + Sinh^{-1}(\frac{q}{2\sqrt{1-2Z}})\frac{Z-(q^2+4(1-2Z))}{q\sqrt{q^2+4(1-2Z)}}\right)\right) \quad (58)$$

and $Z \equiv Z(\mu)$.

The mean-shape at $O(\epsilon)$: Laplace transform in Fourier

Using (26), the mean-shape in Fourier space is computed as $\langle S(q)\rangle_S = \frac{L^d}{\rho^{\mathrm{MF}}(S)}LT^{-1}_{\mu\to S}\left(\tilde{\mathcal{Z}}^{\mathrm{MF}}(\mu,q)\right)$. To order $O(\epsilon)$, we have $\tilde{\mathcal{Z}}(\mu,q) = \tilde{\mathcal{Z}}^{\mathrm{MF}}(\mu,q) + \delta\tilde{\mathcal{Z}}(\mu,q)$. The density ρ was computed to $O(\epsilon)$ in [26] with the result $\rho(S) = \rho^{\mathrm{MF}}(S) + \delta\rho(S)$ with

$$\delta\rho(S) = \alpha\rho^{\mathrm{MF}}(S)\times\frac{\gamma_E(S-6)+4S-8\sqrt{\pi}\sqrt{S}+(S-6)\log(S)+4}{16} \quad (59)$$

$\langle S(q)\rangle_S$ can thus be computed to $O(\epsilon)$ as

$$\langle S(q)\rangle_S = \frac{L^d}{\rho^{\mathrm{MF}}(S)}LT^{-1}_{\mu\to S}\left(\tilde{\mathcal{Z}}^{\mathrm{MF}}(\mu,q)\right) - \frac{L^d\delta\rho(S)}{(\rho^{\mathrm{MF}}(S))^2}LT^{-1}_{\mu\to S}\left(\tilde{\mathcal{Z}}^{\mathrm{MF}}(\mu,q)\right) + \frac{L^d}{\rho^{\mathrm{MF}}(S)}LT^{-1}_{\mu\to S}\left(\delta\tilde{\mathcal{Z}}(\mu,q)\right) + O(\epsilon^2) \;.(60)$$

One can check that the $O(\epsilon^0)$ part of this result allows to retrieve directly the result of the precedent section for the mean-shape (i.e. without computing $\langle v(x,t)\rangle_S$ first), so that everything is consistent. A new difficulty (compared to the BFM case), is that $\langle S(q)\rangle_S$ defined in (60) does not satisfy the scaling form $\langle S(q)\rangle_S = S\tilde{\mathcal{F}}_d(qS^{\frac{1}{d+\zeta}}) \; \forall S$. This is natural: the scaling regime of the problem is for $S \ll S_m$ (here $S_m = 1$ in dimensionless units) and the universal shape of avalanches is the one obtained from (60) as $S \to 0$. It is thus obtained here as

$$\tilde{\mathcal{F}}_d(q) = \lim_{S\to 0}\frac{\langle S(qS^{\frac{-1}{d+\zeta}})\rangle_S}{S} \quad (61)$$

We now compute the ϵ expansion of (61) using (60). By definition $\tilde{\mathcal{F}}_d(q) = \tilde{\mathcal{F}}^{\mathrm{MF}}(q) + \delta\tilde{\mathcal{F}}_d(q)$. We also use the one-loop value of $\zeta = \zeta_1\epsilon$ ($\zeta_1 = 1/3$) and obtain

$$\delta\tilde{\mathcal{F}}_d(q) = \lim_{S\to 0}\epsilon\frac{\zeta_1-1}{16}q\log(S)\frac{\partial\tilde{\mathcal{F}}^{\mathrm{MF}}}{\partial q}(q) + L^d\frac{LT^{-1}_{\mu\to S}\delta\tilde{\mathcal{Z}}(\mu,qS^{-\frac{1}{4}})}{S\rho^{\mathrm{MF}}(S)} - \tilde{\mathcal{F}}^{\mathrm{MF}}(q)\frac{\delta\rho(S)}{\rho^{\mathrm{MF}}(S)} \quad (62)$$

Let us first look at the second term in (62):

$$\begin{aligned}
L^d\frac{LT^{-1}_{\mu\to S}\delta\tilde{\mathcal{Z}}(\mu,qS^{-\frac{1}{4}})}{S\rho^{\mathrm{MF}}(S)} &= \frac{L^d}{S\rho^{\mathrm{MF}}(S)}\int_{c-i\infty}^{c+i\infty}\frac{d\mu}{2i\pi}e^{\mu S}\delta\tilde{\mathcal{Z}}(\mu,qS^{-\frac{1}{4}}) \\
&= \frac{L^d e^{-S/4}}{S\rho^{\mathrm{MF}}(S)}\int_{c'-i\infty}^{c'+i\infty}\frac{d\mu}{2i\pi S}e^{\mu}\delta\tilde{\mathcal{Z}}(-1/4+\mu/S,qS^{-\frac{1}{4}}) \\
&\simeq_{S<<1}\alpha LT^{-1}_{\mu\to 1}\left(H(q,\mu)-\frac{3\sqrt{\pi}}{2}\frac{\sqrt{\mu}\log(S)}{(2\sqrt{\mu}+q^2)^2}+O(S)\right) \quad (63)
\end{aligned}$$

Where here from the first to the second line we used a change of variables $\mu \to -1/4+\mu/S$ and then took the limit $S \to 0^+$ of (58) to define

$$H(q,\mu) = \frac{\sqrt{\mu}\sqrt{\pi}\left(q\left(6\log\left(2\sqrt{\mu}\right)-16\right)\sqrt{8\sqrt{\mu}+q^2}+16\left(9\sqrt{\mu}+q^2\right)\sinh^{-1}\left(\frac{q}{2\sqrt{2}\sqrt[4]{\mu}}\right)\right)}{2q\left(2\sqrt{\mu}+q^2\right)^2\sqrt{8\sqrt{\mu}+q^2}} \quad (64)$$

Using similar manipulations, the other terms are inserted inside the ILT using the representation

$$\tilde{\mathcal{F}}^{\mathrm{MF}}(q) = LT^{-1}_{\mu\to 1}\left(\frac{2\sqrt{\pi}}{2\sqrt{\mu}+q^2}\right) \quad, \quad \frac{\partial\tilde{\mathcal{F}}^{\mathrm{MF}}}{\partial q}(q) = LT^{-1}_{\mu\to 1}\left(\frac{-4\sqrt{\pi}q}{(2\sqrt{\mu}+q^2)^2}\right) \quad, \quad \frac{\zeta_1-1}{16} = \frac{3\alpha}{16\epsilon} \quad (65)$$

This representation shows that the $O(\log(S))$ terms present in (62) cancel and we obtain the result

$$\delta\tilde{\mathcal{F}}_d(q) = \alpha LT^{-1}_{\mu\to 1}\left(-\frac{\sqrt{\pi}}{8}\frac{(4-6\gamma_E)}{(2\sqrt{\mu}+\tilde{q}^2)}+H(q,\mu)\right) \quad (66)$$

which leads to the result (9) in the main text. Note that the result satisfies, as required from normalization

$$\tilde{\mathcal{F}}_d(q=0) = 1 \quad , \quad \delta\tilde{\mathcal{F}}_d(q=0) = 0 \tag{67}$$

which can be checked explicitly from the above expressions using that $LT^{-1}_{\mu\to 1}\frac{\gamma_E + \ln(4\mu)}{\sqrt{\mu}} = 0$. Equivalently, the total shape in Fourier takes the form

$$\tilde{\mathcal{F}}_d(q) = LT^{-1}_{\mu\to 1}\left((1 + \alpha\frac{3\gamma_E - 2}{8})\frac{2\sqrt{\pi}}{q^2 + 2\sqrt{\mu} + \Sigma(q,\mu)}\right) + O(\alpha^2) \tag{68}$$

where the "self-energy" correction reads, to lowest order

$$\Sigma(q,\mu) = -4\alpha\sqrt{\mu}\left(\frac{q^2 + 9\sqrt{\mu}}{q\sqrt{q^2 + 8\sqrt{\mu}}}\sinh^{-1}\left(\frac{q}{2\sqrt{2\sqrt{\mu}}}\right) - 1 + \frac{3}{16}\ln(4\mu)\right) \tag{69}$$

Units and scales: Let us mention here that, since this result was obtained in dimensionless units, the universal scale ℓ_σ appearing in the main text is here given by $\ell_\sigma = \frac{1}{m}\left(\frac{1}{S_m}\right)^{\frac{1}{d+\zeta}}$. S_m can always be measured as $S_m = \frac{\langle S^2\rangle}{2\langle S\rangle}$ and is exactly given in terms of the parameters of the model by $S_m = \frac{\sigma}{m^4}$. As $m \to 0$, the dependence of σ on m is universal: $\sigma \sim m^{4-d-\zeta}\sigma*$ with $\sigma*$ a dimensionless number. Thus $\ell_\sigma \simeq (\sigma*)^{\frac{-1}{d+\zeta}}$. The number $\sigma*$ is non-universal and depends on the microscopic disorder. Thus the scale ℓ_σ is non-universal and depends on *microscopic* properties of the disorder. Note also that using (60) one can also study the dependence of the mean-shape when S gets close to the cutoff avalanche size S_m. This dependence is expected to be non-universal and in our model we find that the amplitude of the $O(\epsilon)$ corrections decrease as S increases close to S_m.

Small and large q expansion of the mean-shape in Fourier space

The small q expansion of $\delta\tilde{\mathcal{F}}_d(q)$ is obtained from (66) at any order. The first terms are:

$$
\begin{aligned}
\delta\tilde{\mathcal{F}}_d(q) \quad &\simeq_{q\ll 1} \alpha\left(-\frac{1}{16}\sqrt{\pi}(-3\gamma_E + 1 + \log(4096))q^2 + \frac{1}{240}(299 - 90\gamma_E)q^4 + \frac{\sqrt{\pi}\alpha(1890\gamma_E - 3121 - 5040\log(2))}{13440}q^6\right. \\
&\left. + \left(\frac{2299}{5040} - \frac{\gamma_E}{8}\right)q^8 + O(q^{10})\right) \\
&\simeq_{q\ll 1} \alpha\left(-0.840378q^2 + 1.02938q^4 - 0.728437q^6 + 0.383999q^8 + O(q^{10})\right)
\end{aligned} \tag{70}
$$

For the large q expansion, the expansion at large q of $\delta\tilde{\mathcal{F}}_d(q)$ cannot be naively ILT. However, since we compute the ILT from μ to 1, one can derive the result with respect to μ any number of times before taking the ILT. This leads to

$$
\begin{aligned}
\delta\tilde{\mathcal{F}}_d(q) \quad &\simeq_{q\gg 1} \alpha\left(\frac{\frac{\gamma_E}{2} + 4 - 4\log(q)}{q^4} - \frac{8\sqrt{\pi}}{q^6} + \frac{-48\gamma_E + 23 - 120\log(q)}{q^8} + \frac{624\sqrt{\pi}}{q^{10}} + O(\frac{1}{q^{12}})\right) \\
&\simeq_{q\gg 1} \alpha\left(\frac{-4\log(q) + 4.28861}{q^4} - \frac{14.1796}{q^6} + \frac{-120\log(q) - 4.70635}{q^8} + \frac{1106.01}{q^{10}} + O(\frac{1}{q^{12}})\right)
\end{aligned} \tag{71}
$$

And as explained in the main text, the first term of this expansion is interpreted as a modification of the power-law behavior of $\tilde{\mathcal{F}}_d(q)$, $\tilde{\mathcal{F}}_d(q) \simeq_{q\gg 1} 2(1 + (2 + \frac{\gamma_E}{4})\alpha)q^{-4-2\alpha} + O(\epsilon^2)$.

Dominant non-analyticity at small x

Let us now understand more precisely how the large q behavior of $\tilde{\mathcal{F}}_d(q)$ generates a non-analyticity in $\mathcal{F}_d(x)$ at small x. We consider the effect of a fat tail $q^{-2\beta}$ in a Fourier transform. We write

$$
\begin{aligned}
\int\frac{d^d q}{(2\pi)^d}\frac{e^{iq_1 x}}{q^{2\beta}} &= \frac{1}{\Gamma(\beta)}\int_{t>0}\frac{dt}{t}t^\beta\int\frac{d^d q}{(2\pi)^d}e^{iq_1 x - q^2 t} = |x|^{2\beta-d}\int dt\frac{2^{-d}\pi^{-\frac{d}{2}}e^{-\frac{1}{4t}}(t)^{\beta-\frac{d}{2}}}{t\Gamma(\beta)} \\
&\sim |x|^{2\beta-d}\frac{2^{-2\beta}\pi^{-\frac{d}{2}}\Gamma\left(\frac{d}{2}-\beta\right)}{\Gamma(\beta)}
\end{aligned} \tag{72}
$$

The above derivation is formal since the integrals in (72) do not converge but we notice that (72) indeed gives, for $\beta = 2$, the dominant non-analyticity in the expansion (42) (i.e. the $b_{p=0}$ term). The above calculation indicates that the leading non-analyticity present in the small x expansion of $\mathcal{F}_d(x)$ is a term of the form

$$\mathcal{F}_d^{sing}(x) \simeq 2(1 + (2 + \frac{\gamma_E}{4})\alpha)|x|^{4+2\alpha-d}\frac{2^{-4-2\alpha}\pi^{-d/2}\Gamma(d/2 - 2 - \alpha)}{\Gamma(2 + \alpha)} \tag{73}$$

Expanding this result in α, it implies the existence of a term

$$\delta\mathcal{F}_d^{sing}(x) \simeq \frac{\alpha}{32}\pi^{-\frac{d}{2}}x^{4-d}\Gamma\left(\frac{d}{2}-2\right)\left(-4\psi\left(\frac{d}{2}-2\right)+8\log(x)+5\gamma_E+4-8\log(2)\right) \tag{74}$$

in the small x expansion of $\delta\mathcal{F}_d(x)$ ($\psi = \frac{\Gamma'}{\Gamma}$ is the diGamma function). For $d=1,3$ this result correctly gives the dominant non-analyticity in $\delta\mathcal{F}_d(x)$. For $d=2$, one has to look at the expansion of (74) around $d=2$. In doing so, one obtains terms (i) regular in x (proportional to x^2) that diverge as $d \to 2$: these terms are unimportant and would be cancelled by other regular terms present in $\delta\mathcal{F}_d(x)$, and (ii) a singular term which admit a well defined $d \to 2$ limit and read:

$$\delta\mathcal{F}_{d=2}^{sing}(x) \simeq \frac{\alpha}{16\pi}(9\gamma_E - 8\log(2) + 4\log(x))x^2\log(x) \;. \tag{75}$$

This term is the dominant non analyticity present in $\delta\mathcal{F}_{d=2}(x)$.

Large x expansion of the mean-shape in real space

We now obtain the modification of the large x behavior of $\mathcal{F}_d(x)$. The mean shape in real space is obtained by Fourier transform and ILT from (i) the expressions $\tilde{\mathcal{F}}^{MF}(q)$ (65), $\delta\tilde{\mathcal{F}}_d(q)$ (66) and the definition of $H(q,\mu)$, (64), or, equivalently to lowest order in α, (ii) from the expressions (68, 69). We use the latter here:

$$\mathcal{F}_d(x) = \int\frac{d^d q}{(2\pi)^d}e^{-iq_1 x}\int_{\mathcal{C}}\frac{d\mu}{2i\pi}e^{\mu}\left(\frac{2\sqrt{\pi}c}{q^2+2\sqrt{\mu}+\Sigma(q,\mu)}\right) \quad, \quad c = (1+\alpha\frac{3\gamma_E-2}{8}) \tag{76}$$

where here the contour $\mathcal{C}$ can be chosen as a wedge around the branch cut $\mu < 0$ of the integrand, such as e.g. $\mathcal{C} = (1+e^{-\frac{3i\pi}{4}}\mathbb{R}_+)\cup(1+e^{\frac{3i\pi}{4}}\mathbb{R}_+)$. To compute this radial Fourier transform, we chose $x > 0$ oriented along the first axis. The integration over the other components $q_2 \ldots q_d$ depends only on $q = \sqrt{q_2^2+\cdots q_d^2}$: the change of variable brings out a factor $S_{d-1} = \frac{2(\pi)^{\frac{d-1}{2}}}{\Gamma(\frac{d-1}{2})}$. Performing the rescaling $(q_1,q) \to \sqrt{2}(q_1,q)$ we obtain the more convenient form

$$\mathcal{F}_d(x/\sqrt{2}) = 2^{\frac{d}{2}}\sqrt{\pi}c\int_{-\infty}^{\infty}\frac{dq_1}{2\pi}\int_0^{\infty}\frac{dqS_{d-1}}{(2\pi)^{d-1}}q^{d-2}e^{-iq_1 x}\int_{\mathcal{C}}\frac{d\mu}{2i\pi}e^{\mu}\frac{1}{q_1^2+q^2+\sqrt{\mu}-\frac{\alpha}{2}h(\sqrt{2}\sqrt{q_1^2+q^2},\mu)} \tag{77}$$

where we denote $\Sigma(q,\mu) = -\alpha\,h(q,\mu)$.

At the mean-field level, i.e. $\alpha = 0$, the integral on q_1 can be performed by closing the contour of integration in the upper half plane (the integrand is then analytic in q_1), and taking into account the contribution of the pole at $q_1(\mu) = i\sqrt{q^2+\sqrt{\mu}}$. The scaling of this pole with μ, $q_1 \sim \mu^{\frac{1}{4}}$ notably leads to the stretched exponential decay of the shape at large x with exponent $4/3$. Here, at $O(\epsilon)$ we cannot a priori performs this residue calculation since the integrand is non analytic in q_1. It seems however reasonable to assume that the behavior of $\mathcal{F}_d(x)$ at large $|x|$ will still be dominated by this pole in the integration on q_1. At first order in $O(\epsilon)$ the position of this pole is shifted as

$$q_1(\mu) \simeq i\left(\sqrt{q^2+\sqrt{\mu}} - \alpha\frac{\delta q(\mu)}{\sqrt{q^2+\sqrt{\mu}}}\right) \quad, \quad \delta q(\mu) = \frac{1}{4}h(i\sqrt{2}\mu^{1/4},\mu) = \frac{1}{72}\sqrt{\mu}\left(27\log\left(2\sqrt{\mu}\right)+14\pi\sqrt{3}-72\right) \tag{78}$$

And for the saddle-point calculation of the integral on q_1, we can approximate

$$\frac{1}{q_1^2+q^2+\sqrt{\mu}-\frac{\alpha}{2}h(\sqrt{2}\sqrt{q_1^2+q^2},\mu)} \simeq \frac{1}{(q_1-q_1(\mu))(q_1+q_1(\mu)-\frac{\alpha}{2}\Delta q(\mu))} \tag{79}$$

With

$$\Delta q(\mu) = \sqrt{2}\sqrt{q^2+\sqrt{\mu}}(\mu)^{-\frac{1}{4}}\partial_1 h(i\sqrt{2}\mu^{\frac{1}{4}},\mu) = \frac{2i}{27}(13\sqrt{3}\pi-63)\sqrt{q^2+\sqrt{\mu}} \tag{80}$$

(Through rescaling one shows that higher order terms in the series expansion of $h(\sqrt{2}\sqrt{q_1^2+q^2},\mu)$ around $q_1 = i\sqrt{q^2+\sqrt{\mu}}$ do not contribute). Hence we have

$$\begin{aligned}
\mathcal{F}_d(x/\sqrt{2}) &= c2^{d/2}\sqrt{\pi}\int\frac{d\mu}{2i\pi}e^{\mu}\int_0^{+\infty}\frac{S_{d-1}}{(2\pi)^{d-1}}q^{d-2}dq\frac{2i\pi}{2\pi}\frac{e^{-x\left(\sqrt{q^2+\sqrt{\mu}}-\frac{\alpha\delta q}{\sqrt{q^2+\sqrt{\mu}}}\right)}}{2q_1(\mu)-\frac{\alpha}{2}\Delta q(\mu)} \\
&\simeq c2^{d/2-1}\sqrt{\pi}\frac{S_{d-1}}{(2\pi)^{d-1}}\int\frac{d\mu}{2i\pi}e^{\mu-x(\mu^{\frac{1}{4}}-\alpha\frac{\delta q}{\mu^{\frac{1}{4}}})}\int_0^{+\infty}q^{d-2}\frac{1}{(1-\frac{\alpha}{54}(13\sqrt{3}\pi-63))\mu^{\frac{1}{4}}-\alpha\frac{\delta q}{\mu^{\frac{1}{4}}}}e^{-x\frac{q^2(\delta q\alpha+\sqrt{\mu})}{2\mu^{3/4}}} \\
&\simeq c\frac{\pi^{1-\frac{d}{2}}}{\sqrt{2}}\int\frac{d\mu}{2i\pi}e^{\mu-xa\mu^b}\frac{1}{a'\mu^b}\left(\frac{a\mu^b}{x}\right)^{\frac{d-1}{2}}
\end{aligned} \tag{81}$$

	$\epsilon = 0$	$\epsilon = 1$	$\epsilon = 2$	$\epsilon = 3$
B at $O(\epsilon)$	$-2/3$	-0.298 ± 0.002	0	0.235 ± 0.014
B conjecture	$-2/3$	-0.2876 ± 0.0001	0	0.100 ± 0.002
δ at $O(\epsilon)$	$4/3$	1.410 ± 0.002	1.49 ± 0.01	1.58 ± 0.02
δ conjecture	$4/3$	1.4246 ± 0.0002	1.570 ± 0.001	1.800 ± 0.004

TABLE I: Predicted values for the exponents B and δ from the $O(\epsilon)$ calculation, and from the conjecture (83) (the values are averaged over the two Pade, and the spread is indicated), and compared to the conjecture (83) using the value of ζ determined numerically in [44] ($\zeta = 0.355 \pm 0.001$ for $d = 3$ and $\zeta = 0.753 \pm 0.002$ for $d = 2$) and [45] ($\zeta = 1.250 \pm 0.005$ in $d = 1$).

Where we have used the fact that the dominant behavior of the integral on q is given by $q \simeq 0$, and we have introduced the notation

$$a = 1 + \frac{-14\sqrt{3}\pi + 72 - 9\log(8)}{72}\alpha \quad , \quad b = \frac{1}{4} - \frac{3}{16}\alpha \quad , \quad a' = 1 + \frac{468 - 94\pi\sqrt{3} - 81\log(2)}{216}\alpha \qquad (82)$$

So that $a\mu^b = \mu^{\frac{1}{4}} - \alpha\frac{\delta q}{\mu^{\frac{1}{4}}} + O(\epsilon^2)$ and $a'\mu^b = (1 - \frac{\alpha}{54}(13\sqrt{3}\pi - 63))\mu^{\frac{1}{4}} - \alpha\frac{\delta q}{\mu^{\frac{1}{4}}} + O(\alpha^2)$. Note that, using $\zeta = \frac{1}{3}\epsilon$ and $\alpha = -2\epsilon/9$, the $O(\epsilon)$ value of b is consistent with the conjecture $b = \frac{1}{d+\zeta}$ which is quite natural: the exponent b gives the scaling with μ of the pole $q_1(\mu) \sim \mu^b$. We know that momenta inside avalanches of sizes S scale with S as $S^{\frac{-1}{d+\zeta}}$. On the other hand, μ is conjugate to S: $\mu \sim S^{-1}$, hence the conjecture $q_1(\mu) \sim \mu^{\frac{1}{d+\zeta}}$. At large x, the integral on μ can now be evaluated using a saddle-point calculation. It leads to, at first order in ϵ,

$$\mathcal{F}_d(x) \simeq Ax^B e^{-Cx^\delta}$$

$$A = \frac{2^{-d/2}\pi^{\frac{1}{2}-\frac{d}{2}}}{\sqrt{3}}\left(1 + \frac{1}{216}\alpha\left(4\sqrt{3}\pi(27 - 7d) + 9(13d + 9(\gamma_E - 8))\right)\right)$$

$$B = -\frac{d-2}{2}\frac{1-2b}{1-b} = \frac{2-d}{3}\left(1 + \frac{1}{2}\alpha\right)$$

$$C = \frac{3}{4} + \alpha\frac{(36 - 7\sqrt{3}\pi)}{36} \quad , \quad \delta = \frac{1}{1-b} = \frac{4}{3} - \frac{\alpha}{3}$$

Following the conjecture on the value of b we can also conjecture

$$B = -\frac{(d-2)(d+\zeta-2)}{2(d+\zeta-1)} \quad , \quad \delta = \frac{d+\zeta}{d+\zeta-1} \qquad (83)$$

Setting $\alpha = 0$ in the above result, we retrieve the large x behavior of $\mathcal{F}_d^{\mathrm{MF}}(x)$ using here a totally different route. Lets us warn the reader that there is some uncertainty on the values of A and B since additional contributions could come from the branch cut in q_1. The values of C and δ however should be correct. The resulting numerical values of the exponents B and δ are summarized in Table I.

Note that (83) can also be expanded in α and gives the prediction

$$\delta\mathcal{F}_d(x) \simeq_{x>>1} \alpha\frac{2^{-\frac{d}{2}-3}\pi^{\frac{1}{2}-\frac{d}{2}}e^{-\frac{3}{4}x^{4/3}}x^{\frac{2}{3}-\frac{d}{3}}}{27\sqrt{3}}\left(2\pi\sqrt{3}\left(-14d + 21x^{4/3} + 54\right)\right.$$

$$\left. + 9\left(\left(-4d + 6x^{4/3} + 8\right)\log(x) + 13d - 24\left(x^{4/3} + 3\right) + 9\gamma\right)\right) \qquad (84)$$

Numerical obtention of the mean shape

The correction $\delta\tilde{\mathcal{F}}_d(q)$ can easily be obtained numerically using a numerical integration on the formula (66) and choosing a contour of integration for μ as $\mathcal{C} = (1 + e^{-\frac{3i\pi}{4}}\mathbb{R}_+) \cup (1 + e^{\frac{3i\pi}{4}}\mathbb{R}_+)$. The precision of the numerical integration can be tested against the exact results at small and large q, (see Fig. 6). It can easily be Fourier transformed in any dimension to find the correction $\delta\mathcal{F}_d(x)$:

$$\delta\mathcal{F}_{d=1}(x) = 2\int_0^\infty \frac{dq}{2\pi}\cos(qx)\delta\tilde{\mathcal{F}}_d(q) \quad , \quad \delta\mathcal{F}_d(x) = \frac{1}{(2\pi)^{\frac{d}{2}}x^{\frac{d-2}{2}}}\int_0^\infty dq J_{\frac{d-2}{2}}(qx)q^{\frac{d}{2}}\delta\tilde{\mathcal{F}}_d(q) \qquad (85)$$
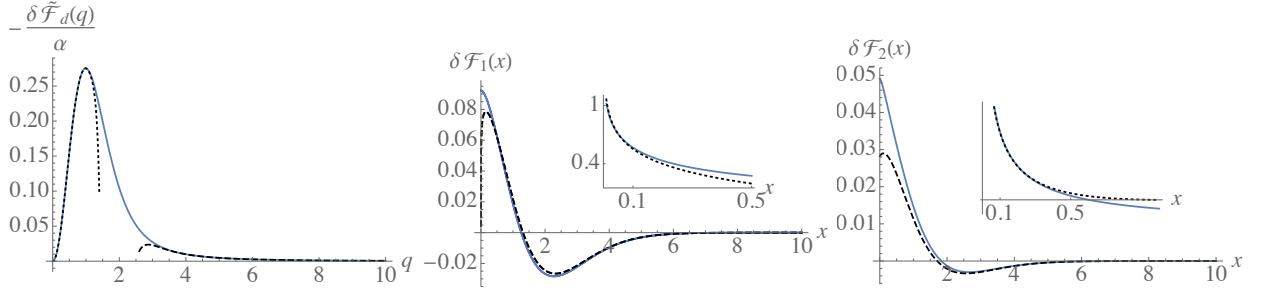
FIG. 6: In blue from left to right: $O(\epsilon)$ correction to the mean-shape in Fourier space divided by $-\alpha$, $-\frac{\delta\tilde{\mathcal{F}}_d(q)}{\alpha}$, in real space in $d = 1$, $\delta\mathcal{F}_1(x)$ and in $d = 2$, $\delta\mathcal{F}_2(x)$. The dotted line on the left is the theoretical small q expansion (70) up to $O(q^{20})$ and the dashed line is the large q expansion (71). The dashed line in the middle and on the right are the theoretical large x expansion (84). Middle inset: plot of $\frac{1}{x^3}\left(\delta\mathcal{F}_1(0) - \delta\mathcal{F}_1(0) - \frac{a_0}{2}x^2\right)$ (plain line), compared with the prediction (74) (dashed line). Right inset: plot of $-\frac{\delta\mathcal{F}_2(x)-\delta\mathcal{F}_2(0)+0.06x^2}{x^2}$ (plain line), compared with the prediction (75) (dashed line).

where $J_n(x)$ denotes the Bessel function of the first kind. The large x behavior of these corrections agrees with our prediction (84), to a surprisingly large extent (see Fig. 6). Some properties of these corrections are their values at the origin $\delta\mathcal{F}_{d=1}(0) = 0.09227$, $\delta\mathcal{F}_{d=2}(0) = 0.04912$, the position where they cross 0, $x_0 = 1.2567$ ($d = 1$), $x_0 = 1.8286$ ($d = 2$), the position of their minimum and minimal value, $x_{min} = 2.2783$, $\mathcal{F}_1(x_{min}) = -0.02835$, $x_{min} = 2.6634$; $\mathcal{F}_2(x_{min}) = -0.002980$ ($d = 2$). We also investigate the presence of non-analyticities in the form of logarithm in the short-distance behavior of the result. In dimension 1, the correction $\delta\mathcal{F}_1(0)$ has a second derivative at 0 evaluated as $a_0 = \delta\mathcal{F}_1''(0) \simeq -0.512$. By plotting $\frac{1}{x^3}\left(\delta\mathcal{F}_1(0) - \delta\mathcal{F}_1(0) - \frac{a_0}{2}x^2\right)$, we shed the light on the non analyticity present in $\delta\mathcal{F}_1(x)$ at small x, which is found to be in very good agreement with (74) (see Fig. 6). In dimension 2, the dominant non-analyticity predicted in (75) compares very well with the plot of $\frac{\delta\mathcal{F}_2(x)-\delta\mathcal{F}_2(0)+0.06x^2}{x^2}$ at small x (the $0.06x^2$ term is a regular term which was not predicted by our calculations).

Adding naively these corrections to the mean-field result $\mathcal{F}_d(x) = \mathcal{F}_d^{\text{MF}}(x) + \delta\mathcal{F}_d(x)$ then gives a result which suffers from several problems. At large x it becomes slightly negative in $d = 1$ and does not have the right non-analytic behavior at small x. The second problem can be cured by considering the reexponentiated Fourier result

$$\tilde{\mathcal{F}}_d^{\text{reg}}(q) = \tilde{\mathcal{F}}_d^{\text{MF}}(q)\exp\left(\frac{\delta\tilde{\mathcal{F}}_d(q)}{\tilde{\mathcal{F}}_d^{\text{MF}}(q)}\right) \tag{86}$$

This result is still correct to first order in ϵ and has the advantage of having the correct behavior at large q, $\tilde{\mathcal{F}}_d^{\text{reg}}(q) \simeq 2(1 + (2 + \frac{\gamma_E}{4})\alpha)q^{-4-2\alpha} + O(\epsilon^2)$. It is plotted in plain red in Fig. 7. Taking the Fourier transform of this result we obtain a function $\mathcal{F}_d^{\text{reg1}}(x)$ which has now the correct behavior at small x but is still slightly negative at large x. On the other hand the function

$$\mathcal{F}_d^{\text{reg2}}(x) = \frac{1}{\mathcal{N}}\exp\left(-\exp\left(\log(-\log(\mathcal{F}_d^{\text{MF}}(x))) + \frac{\delta\mathcal{F}_d(x)}{\mathcal{F}_d^{\text{MF}}(x)\log(\mathcal{F}_d^{\text{MF}}(x))}\right)\right) \tag{87}$$

where $\mathcal{N}$ is a normalization constant ensuring that $\int d^d x\, \mathcal{F}_d^{\text{reg2}}(x) = 1$, is correct to $O(\epsilon)$ and takes properly into account the change of exponent in the exponential decay of the shape at $x = \infty$ and is everywhere positive. However, it doesn't have the correct behavior at small x. Since $\mathcal{F}_d^{\text{reg1}}(x)$ and $\mathcal{F}_d^{\text{reg2}}(x)$ intersect themselves at some x_c, we construct the function

$$\mathcal{F}_d^{\text{reg}}(x) = \frac{1}{\mathcal{N}}\left(r(x)\mathcal{F}_d^{\text{reg1}}(x) + (1 - r(x))\mathcal{F}_d^{\text{reg1}}(x)\right) \tag{88}$$

where $\mathcal{N}$ is a normalization factor and $r(x)$ is a function that interpolates smoothly between $r(1) = 1$ and $r(\infty) = 0$ sufficiently fast to obtain a positive result everywhere. Here we have chosen $r(x) = e^{-x^2/xc^2}$ but this choice does not matter drastically since all these functions are close to each others (see Fig. 7). The result (88) is still correct to $O(\epsilon)$ and has the right behavior at small and large x. It is plotted for $d = 1$ and $d = 2$ in plain red in (7) and used for comparison to numerical simulations.
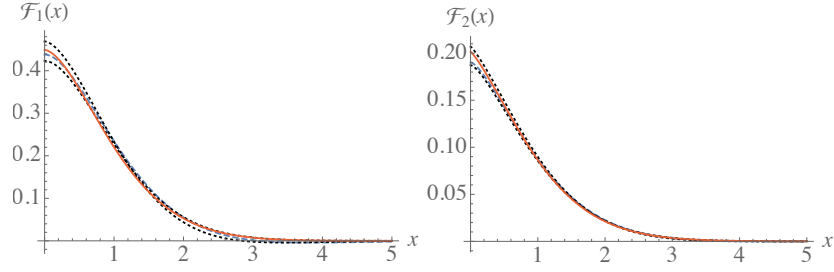
FIG. 7: Different mean shape $\mathcal{F}_d(x)$ correct at $O(\epsilon)$ for $d = 1$ (left) and $d = 2$ (right). Dashed-blue lines: naive result $\mathcal{F}_d(x) = \mathcal{F}_d^{\mathrm{MF}}(x) + \delta\mathcal{F}_d(x)$. Dotted lines: $\mathcal{F}_d^{\mathrm{reg1}}(x)$ (largest at the origin) and $\mathcal{F}_d^{\mathrm{reg2}}(x)$ (smallest at the origin). Red line: regularized result $\mathcal{F}_d^{\mathrm{reg}}(x)$ used for comparison with numerics.

	c_1	c_2	c_3	c_4	c_5	c_6
Gaussian $d = 1$	1.5708	3	5.8905	11.67	29.1938	46.2
BFM $d = 1$: Theory	1.6944	3.8197	9.2703	23.3333	60.045	156.863
SR $d = 1$: Theory	1.6944	3.8197	9.2703	23.3333	60.045	156.863
	$+0.0798\alpha$	$+0.6196\alpha$	$+2.8\alpha$	$+11.4444\alpha$	$+37\alpha$	$+138.296\alpha$
	$\simeq 1.641$	$\simeq 3.43$	$\simeq 7.53$	$\simeq 16.6$	$\simeq 38.5$	$\simeq 81$
	± 0.001	± 0.02	± 0.16	± 0.9	± 3.7	± 17
Gaussian $d = 2$	1.27324	2	3.3953	6	10.865	20
BFM $d = 2$: Theory	1.3734	2.5464	5.3435	12	28.1289	67.9111
SR $d = 2$: Theory	1.3734	2.5464	5.3435	12	28.1289	67.9111
	$+0.06482\alpha$	$+0.4110\alpha$	$+1.6647\alpha$	$+5.7758\alpha$	$+18.6579\alpha$	$+58.0856\alpha$
	$\simeq 1.3449$	$\simeq 2.369$	$\simeq 4.65$	$\simeq 9.6$	$\simeq 20.8$	$\simeq 45.7$
	± 0.0002	± 0.006	± 0.05	± 0.2	± 0.9	± 3.6

TABLE II: Prediction for the universal ratios in dimension 1 ($\epsilon = 3$) and 2 ($\epsilon = 2$). Here $\alpha = -2\epsilon/9$. The values displayed are the average over the two Pade and their spread is indicated (as an indication of the uncertainty).

Universal ratios

Here we compute the universal ratios in dimension 1 and 2 of the various mean-shapes. These are defined as $c_p = \frac{\int d^d x |x|^{2p} \mathcal{F}_d(x)}{(\int d^d x |x|^p \mathcal{F}_d(x))^2}$. In dimension 1 and for p even they are exactly obtained as $c_p = \frac{\tilde{\mathcal{F}}_d^{(2p)}(0)}{\left(\tilde{\mathcal{F}}_d^{(p)}(0)\right)^2}$. For p odd and in dimension $d = 2$ one has to rely on direct numerical integration techniques. Fortunately, the exponential decay of the shape at large x (which is known analytically) allows us to obtain an excellent numerical precision, we compute them pertubatively in $O(\epsilon)$ using

$$c_p \simeq \frac{\int d^d x |x|^{2p} \mathcal{F}_d^{\mathrm{MF}}(x)}{\left(\int d^d x |x|^p \mathcal{F}_d^{\mathrm{MF}}(x)\right)^2} + \alpha \left(\frac{\int d^d x |x|^{2p} \delta\mathcal{F}_d(x)}{\left(\int d^d x |x|^p \mathcal{F}_d^{\mathrm{MF}}(x)\right)^2} - 2 \frac{\int d^d x |x|^{2p} \mathcal{F}_d^{\mathrm{MF}}(x) \int d^d x |x|^p \delta\mathcal{F}_d(x)}{\left(\int d^d x |x|^p \mathcal{F}_d^{\mathrm{MF}}(x)\right)^3} \right) \tag{89}$$

Table II contains our results in $d = 1$ and $d = 2$. The even values in $d = 1$ are exact for both the BFM and (to $O(\epsilon)$) the SR case. The odd values are results of numerical integration. The uncertainty on the numerical integration is evaluated in $d = 1$ by comparing the result obtained using numerical integrations for even ratios to the exact ones. The values in $d = 2$ are results of numerical integrations. We also give for reference in Table II the value of the universal ratios for a Gaussian shape function ($\mathcal{F}_{d=1}^{\mathrm{Gauss}}(x) = \frac{e^{-x^2}}{\sqrt{\pi}}$ and $\mathcal{F}_{d=2}^{\mathrm{Gauss}}(x) = \frac{e^{-x^2}}{\pi}$)

Details on numerical simulations

Parameters of the simulations

For our simulations we have used $\sigma = 1$ and $dt = 0.02$. The discretization in time is handled using an algorithm similar to the one presented in [46]. The used values of δw and number of simulated kicks n_{kicks} are: $\delta w = 0.1$ and $n_{kicks} = 40 \times 10^6$ for the SR model; $\delta w = 1$ and $n_{kicks} = 100 \times 10^6$ for the BFM model. As discussed in the main text, these simulations are performed in $d = 1$ for a line of size $L = 2048$ discretized with $N = L$ points. For the SR model, δu is chosen as $\delta u = 5\delta w$.
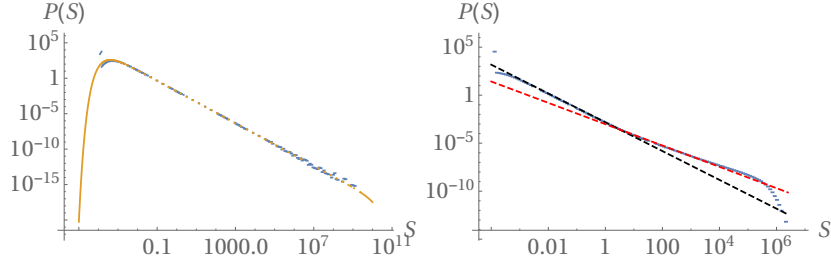
FIG. 8: Blue: Measurement of the avalanche size distribution in the BFM model (left) and the SR model (right). Yellow curve on the left: theoretical prediction for $P(S) = p^{\mathrm{MF}}(S)$ (no scaling parameter). The excess of small avalanches is an artifact due to the discretization and does not affect the statistics of larger avalanches. Black dashed line on the right: power-law $S^{-\tau_S^{\mathrm{BFM}}}$ with $\tau_S^{\mathrm{BFM}} = 3/2$. Red dashed line on the right: power-law $S^{-\tau_S^{\mathrm{SR}}}$ with $\tau_S^{\mathrm{SR}} \simeq 2 - \frac{2}{1+1.250} \simeq 1.11$.

PDF of avalanche sizes and measurement of S_m

The measurement of the PDF $P(S)$ (plotted in Fig. 8) shows that the avalanche size distribution of both models have a lower cutoff $S_{\delta w} \simeq \frac{(L^d \delta w)^2}{S_m^{\mathrm{BFM}}}$ where S_m^{BFM} is always given by σ/m^4. In the BFM model, we observe a scaling regime $P(S) \sim S^{-\tau_S^{\mathrm{BFM}}}$ with $\tau_S^{\mathrm{BFM}} = 3/2 = 2 - \frac{d}{d+\zeta^{\mathrm{BFM}}}$ ($\zeta^{\mathrm{BFM}} = 4 - d$) for $S_{\delta w} \ll S \ll S_m^{\mathrm{BFM}}$. In the SR model, for $S_{\delta w} \leq S \leq S_{\delta u} = S_{\delta u} \simeq (\delta u)^{\frac{d+\zeta^{BFM}}{\zeta^{BFM}}}$, the interface does not feel the short-ranged nature of the disorder and we observe a first scaling regime coherent with the BFM, $P(S) \sim S^{-\tau_S^{\mathrm{BFM}}}$. In the SR model, S_m^{SR} is measured as $\langle S^2 \rangle / (2\langle S \rangle)$ with the result $S_m^{\mathrm{SR}} = (1.40 \pm 0.05) \times 10^5$ (statistical uncertainty given with 3 sigma estimation). For $S_{\delta u} \ll S \ll S_m^{\mathrm{SR}}$, we observe a second scaling regime coherent with the known features of the SR fixed point: $P(S) \sim S^{-\tau_S^{\mathrm{SR}}}$ with $\tau_S^{\mathrm{SR}} = 2 - \frac{d}{d+\zeta^{\mathrm{SR}}}$ and our data are consistent with the value of ζ numerically estimated in [45], $\zeta^{\mathrm{SR}} \simeq 1.250 \pm 0.005$ (see Fig. 8). These measurements allows us to identify the desired scaling regime and compare our simulations with known features of the BFM and SR fixed point.

Details on the search for the seed

Let us now make a few comments on some subtle points and emphasize the importance of the algorithm used in the main text to retrieve the seed of each avalanche. When we apply a uniform kick of size δw to the system, the interface always moves from a small amount. As seen above and in Fig. 8, avalanches of size much smaller than $S_{\delta w}$ are very unlikely (note that the discretization procedure introduces another sharp, artificial, small scale cutoff on the avalanches size: since each points moves at least during the first iteration of the algorithm with velocity $m^2 \delta w / \eta$, the avalanche cannot be smaller than $L^d dt m^2 \delta w / \eta$). After the first iteration, it is actually highly probable that several points along the interface are still moving, each of them being the seed of an avalanche. With a high probability, these small avalanches have sizes of order $S_{\delta w}$ and quickly perish, hence we do not analyze their shapes (they are 'microscopic avalanches'). In the following we are only interested in the shape of avalanches of total size $S > 1 \gg S_{\delta w}$ ('macroscopic avalanches'), which only occur with a small probability. When such an avalanche occurs, since there is a large separation of scales with the small avalanches of order $S_{\delta w}$, we expect its shape to be only very weakly perturbed by the fact that other small avalanches could have been triggered after the kick. We neglect the small probability that more than one macroscopic avalanche have been triggered by the kick. A crucial step is to unambiguously identify, from the set of points still moving during the second iteration of the algorithm, which one is the true seed of the observed macroscopic avalanche. This is what is accomplished by the algorithm explained in the text: after n_t iterations of the algorithm, all the small avalanches triggered at the beginning of the avalanche have already stopped (thus in general n_t has to be chosen sufficiently large). Identifying the maximum velocity inside the avalanche at time n_t, we are sure to have identified a point which is inside the macroscopic avalanche. The algorithm is then devised to run within the history of the avalanche backward in time and always identify a point moving along the interface *which is in the correct cluster of moving points defining the macroscopic avalanche*. This is illustrated in Fig. 9

Measurement of the mean-shape

We always only measure mean-shape with values of S well inside the desired scaling regime. The binning on the values of the total size S is of 0.05, we construct a grid of total sizes with the values $S_i = 1 \times \left(\frac{1.05}{0.95}\right)^{i-1}$ and avalanches with total size S such that $0.95 S_i < S < 1,05 S_i$ are rescaled as $S \to S_i$. The difference between S_m^{SR} and S_m^{BFM} and τ_S^{SR} and τ_S^{BFM} explains the difference between the chosen values of δw and n_{kicks} for each model: these parameters are adjusted so as to give a comparable numerical precision for the measurement of the mean-shape of interest (i.e. large avalanches which provide a good spatial precision - for the same δw, one observes more large avalanches in the
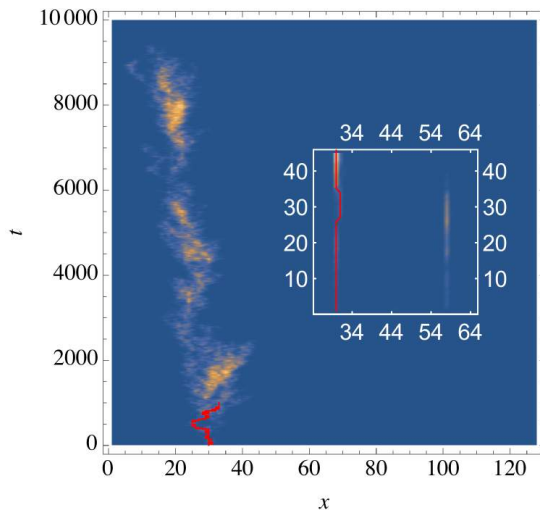
FIG. 9: Density plot of the velocity field $v(x,t)$ inside an avalanche of size $S = 1760$ in the mean-field model (BFM) for $d = 1$ discretized with $N = 128$ points. Line in red: backward path produced by the algorithm to find the seed of the avalanche. The inset illustrates the efficiently of the algorithm to identify, from the set of moving points of the interface just after the kick, the true seed of the observed macroscopic avalanche. In this avalanche (at least) two points (at $x = 32$ and $x = 57$) still moves at $t = 2dt$, but only the point at $x = 32$ is inside the cluster of moving points of the macroscopic avalanche and can be its seed.
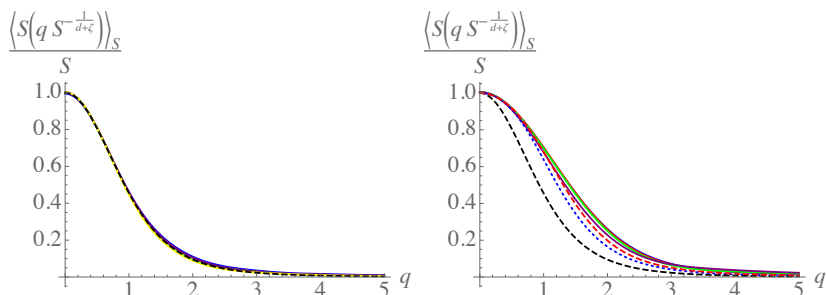

FIG. 10: The mean shape in Fourier space measured in simulations (left: BFM and right:SR), (plain lines, same color code as Fig. 4) and compared to the theoretical predictions (dashed-black: BFM result, dotted-blue: naive $O(\epsilon)$ result and dashed-red: improved $O(\epsilon)$ result (86).

SR model than in the BFM model). The shapes are rescaled onto one another using the value of ζ given above and determined numerically in [45]. The fact that they collapse (see Fig. 4) using this value is another check that our simulations are correct since they appear in agreement with the high-precision simulations performed in [45]. Let us also present here the results analogous to Fig. 4 in Fourier space: see Fig. 10.

Measurement of the non-analyticity at small x and fat tail at large q

To measure these observables with a good precision in $d = 1$, we use the models discretized using 2048 points. We first obtain a smooth numerical mean-shape for the BFM and SR model by taking the average of several mean-shapes obtained for various sizes (taken large to obtain a good spatial precision: for the BFM we use 20 shapes with $13575 < S < 100478$, for the SR model we use 10 shapes with $7386 < S < 20095$). The resulting shapes are shown on the left of Fig. 11. We also plot in Fig. 12 the difference between the mean shape measured in our numerical simulations of the SR model and the theoretical mean-field result in $d = 1$ and compare it with our theoretical $O(\epsilon)$ predictions. This notably highlights the efficiency of the reexponentiation procedure discussed previously. We then directly study the small x behavior of these shapes, leading to the results presented on the left of Fig. 5. The study of the large q behavior is more tedious: at large x the mean shapes we obtained start to be dominated by the noise present in our numerical results. This noise blurs the analysis of the large frequency content of the mean-shape. We thus first smooth our results at large x result by using an exponential fit e^{-Cx^δ} with the theoretical value of δ previously obtained exactly for the BFM and using our conjecture (83) for the SR model (see Table I). This fitting procedure is illustrated in Fig. 11. By Fourier transform, we then obtain the results presented on the right of Fig. 5.
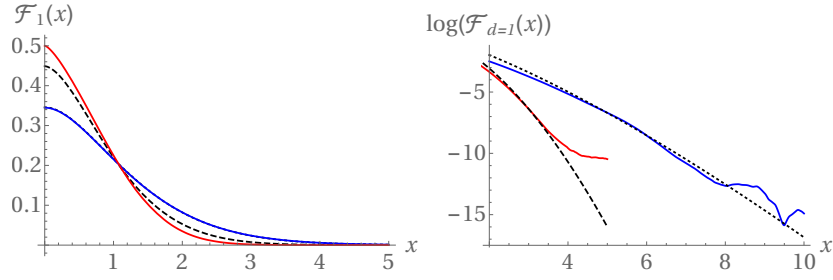
FIG. 11: Left: mean shapes obtained in the simulations of the SR model (red) and of the BFM model (blue) compared with the $O(\epsilon)$ result (dashed, black) and BFM result (dotted black). Right: blue (resp. red) large x behavior of the mean shape measured in the BFM model (resp. SR model). To avoid the noise present at large x to dominate the large q behavior of the mean shape, we smooth our result at large x using an exponential ansatz as explained below.
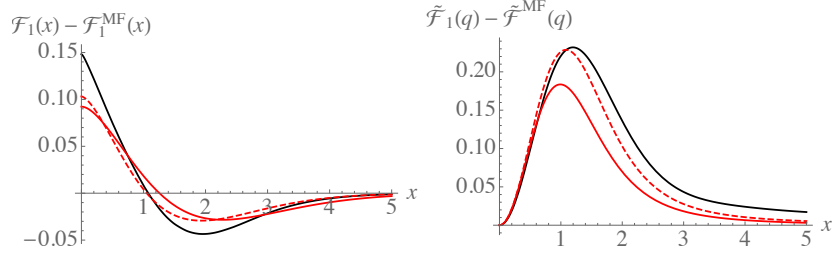

FIG. 12: Left: (resp. Right:) Black line: Difference between the mean shape measured in the numerical simulations of the SR model in real space $\mathcal{F}_1(x)$ (resp. in Fourier space $\tilde{\mathcal{F}}_1(q)$) and the theoretical mean field result $\mathcal{F}_1^{\mathrm{MF}}(x)$ (44) (resp. $\tilde{\mathcal{F}}^{\mathrm{MF}}(q)$ (5)). Red line: theoretical $O(\epsilon)$ result $\delta\mathcal{F}_1(x)$ (85) (resp. $\delta\tilde{\mathcal{F}}_1(q)$ (66)). Red-dashed line: improved (through the reexponentiation procedure) theoretical $O(\epsilon)$ result $\mathcal{F}_1^{\mathrm{reg}}(x) - \mathcal{F}_1^{\mathrm{MF}}(x)$ (88) (resp. $\tilde{\mathcal{F}}_1^{\mathrm{reg}}(q) - \tilde{\mathcal{F}}^{\mathrm{MF}}(q)$ (86)). The reexponentiation procedure chosen in Fourier space sensibly improves the accuracy of the result. Nevertheless, higher loop corrections will be necessary to account for the remaining difference.

Measurement of the universal ratios

Here we describe the protocol used to measure the universal ratios. We measure the universal ratios defined in (89) using severall cutoff length ℓ_{cut} for the integral on x (i.e. we consider different approximations of the universal ratios $c_j(\ell_{cut}) = \frac{\int_{-\ell_{cut}}^{\ell_{cut}} dx |x|^{2p} \mathcal{F}_1(x)}{\left(\int_{-\ell_{cut}}^{\ell_{cut}} dx |x|^p \mathcal{F}_1(x)\right)^2}$ that should converge to the true universal ratios c_j as $\ell_{cut} \to \infty$). These are measured on the mean-shape $\mathcal{F}_1(x)$ numerically obtained for each possible total size S_i (see above for the definition of the binning procedure). Using these measurements we make sure that ℓ_{cut} is chosen large enough so that the results are not sensitive to its finite value. We also control discretization artifacts by studying the dependence of the measured universal ratios $c_j(\ell_{cut})$ on the total size S_i: for small S_i, the avalanches extend only over a few sites and the mean shape deduced from them is different from the one of the continuum theory, a difference that is seen in the universal ratios. For large enough S_i, the universal ratios become size independent and we reach the continuum regime. This is illustrated for the two first universal ratios in the BFM model in Fig. 13. In the end, the universal ratios are measured by performing an average over various, large enough total sizes S_i, leading to the values presented in Table III.

	c_1	c_2	c_3	c_4	c_5	c_6
BFM $d=1$: Theory	1.694	3.819	9.270	23.334	59.255	156.863
SR $d=1$: Theory	$\simeq 1.641$ ± 0.001	$\simeq 3.43$ ± 0.02	$\simeq 7.53$ ± 0.16	$\simeq 16.6$ ± 0.9	$\simeq 38.5$ ± 3.7	$\simeq 81$ ± 17
BFM $d=1$: Numerics	1.699 ± 0.003	3.83 ± 0.05	9.3 ± 0.3	23 ± 7	59 ± 26	143 ± 41
SR $d=1$: Numerics	1.612 ± 0.004	3.16 ± 0.03	6.4 ± 0.3	13.6 ± 0.2	27 ± 2	57 ± 9

TABLE III: Universal ratios in dimension 1. First two lines: theoretical result for the BFM and $O(\epsilon)$ theoretical result for the SR universality class. Last two lines: numerical measurement in the simulations of the BFM and SR model. Error-bars for the numerics are 3-sigma estimates.
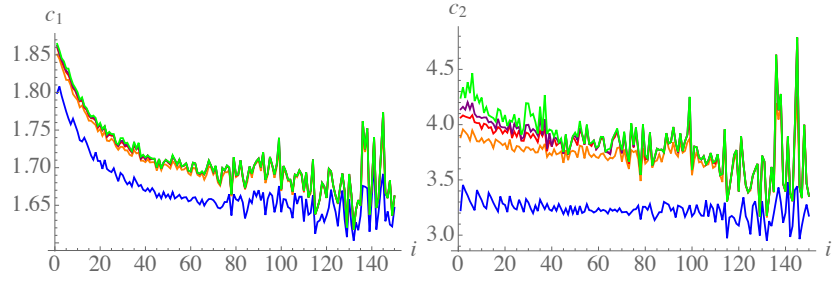
FIG. 13: Universal ratios $c_1(\ell_{cut})$ (left) and $c_2(\ell_{cut})$ (right) measured in the BFM for various cutoff length $\ell_{cut} = 4, 6, 8, 10, 12$ (Blue, Orange, Red, Purple and Green) as a function of the total sizes $S = S_i = 1 \times (\frac{1.05}{0.95})^{i-1}$. For the BFM, as a consequence of these plots, the results presented in Table III are averages on the universal ratios obtained for $S > S_i$ with $i = 60$ and $\ell_{cut} = 8$ to obtain a result that do not depend on ℓ_{cut} and is free of discretization artifacts as explained in the text. A similar procedure is used for the SR model. Note that the important variations observed here for large i are just a consequence of the fact that only a few avalanches with the largests S_i have been measured, hence the statistical uncertainty on the measurements of $c_i(\ell_{cut})$ increases when S_i increases.